Physiological Response of Penicillium chrysogenum to Mimicked Local and Global Perturbations of Substrate and Dissolved Oxygen Gradients at Industrial-Scale

Chen, Yining; Haringa, Cees; Wang, Zejian; Zhuang, Yingping; Wang, Guan

DOI
10.1002/bit.28968

Publication date
2025

Document Version
Final published version

Published in
Biotechnology and Bioengineering

Citation (APA)
Chen, Y., Haringa, C., Wang, Z., Zhuang, Y., & Wang, G. (2025). Physiological Response of Penicillium chrysogenum to Mimicked Local and Global Perturbations of Substrate and Dissolved Oxygen Gradients at Industrial-Scale. *Biotechnology and Bioengineering*, *122*(6), 1402-1423. https://doi.org/10.1002/bit.28968

Biotechnology and Bioengineering

WILEY

BIOTECHNOLOGY AND BIOENGINEERING

ARTICLE

Physiological Response of *Penicillium chrysogenum* to Mimicked Local and Global Perturbations of Substrate and Dissolved Oxygen Gradients at Industrial-Scale

Yining Chen[1] | Cees Haringa[2] | Zejian Wang[1] | Yingping Zhuang[1,3] | Guan Wang[1,3]

[1]State Key Laboratory of Bioreactor Engineering, East China University of Science and Technology (ECUST), Shanghai, People's Republic of China | [2]Department of Biotechnology, Delft University of Technology, Delft, the Netherlands | [3]Qingdao Innovation Institute of East China University of Science and Technology, Shanghai, People's Republic of China

Correspondence: Guan Wang (guanwang@ecust.edu.cn)

Received: 18 September 2024 | **Revised:** 24 December 2024 | **Accepted:** 26 February 2025

Funding: This study was supported by National Key Research and Development Program of China (2021YFC2101000), National Natural Science Foundation of China (31900073, 21978085), Shanghai Rising-Star Program (21QA1402400), Natural Science Foundation of Shanghai Municipality (19ZR1413600), and Fundamental Research Funds for the Central Universities (JKF01241708).

Keywords: dissolved oxygen gradients | industrial-scale fermentation | metabolomics | *Penicillium chrysogenum* | scale-down | substrate gradients

ABSTRACT

Industrial-scale microbial fermentation processes often face limitations in mixing and mass transfer, leading to the formation of environmental gradients within the bioreactor. These gradients expose microbes to heterogeneous conditions over time and space. In this study, we evaluated the effects of combined substrate and dissolved oxygen (DO) gradients on the metabolic response of *Penicillium chrysogenum* at an industrial scale. Three representative heterogeneous environments were simulated in scale-down systems: (1) feed inlet (high glucose, low oxygen (HGLO): $C_S > 20$ mM, DO < 0.012 mM), (2) aeration inlet (high oxygen, low glucose (HOLG): $C_S < 0.8$ mM, DO > 0.2 mM), and (3) global environment (periodic 360 s fluctuation cycle with 45 s of HGLO and 75 s of HOLG conditions). Results showed that prolonged exposure to feed inlet conditions led to a complete loss of penicillin production capacity, accompanied by significant excretion of intracellular metabolites, and this effect was largely irreversible. While, cells randomly walking under the top impeller zone did not lose production capacity but showed signs of premature degeneration due to increased energy demand. When exposed to the global environment, cells finely tuned their metabolism in a periodical manner, with nearly a 50% loss of penicillin productivity. In summary, substrate gradients alone did not cause irreversible effects, but large substrate gradients contributed to reduced productivity. Oxygen gradients, however, not only reduced production but also caused irreversible cellular damage. These findings provide valuable insights for developing scale-up criteria and strain engineering strategies aimed at improving large-scale culture performance.

1 | Introduction

The global biotechnology market value is projected to reach 2–4 trillion USD between 2030 and 2040 (Kampers et al. 2021), driven by increasing demand for bio-based products. This growth underscores the need for large-scale, efficient bioreactor systems (Wang et al. 2020). However, scaling biotechnological processes from the laboratory to industrial levels often encounters the "scale-up effect", resulting in a 10%–30% reduction in key metrics such as titer, rate, and yield (T.R.Y.) and, in some cases, complete batch failures (Olughu et al. 2019). This challenge is primarily attributed to the disparity between laboratory-scale proof-of-principle and industrial-scale processes (Linton and Xu 2021). As bioreactor volume increases, limitations in mixing and mass

transfer become more pronounced. In large-scale reactors (over 100 m^3), mixing times can extend to tens or even hundreds of seconds, while cellular metabolic response times typically remain in the range of seconds to tens of seconds (G. Wang et al. 2015). When mixing times exceed cellular response times, significant environmental gradients (e.g., substrate, pH, dissolved oxygen, and CO_2) can develop, complicating process control and reducing efficiency (Nadal-Rey, McClure, Kavanagh, Cornelissen, et al. 2021).

In such heterogeneous environments, cells are continuously exposed to fluctuating conditions as they move through different regions of the bioreactor (Haringa et al. 2016). In large-scale practices, prolonged exposure to these fluctuating environments may trigger overflow metabolism, often leading to by-product accumulation and a decrease in production capacity (Nadal-Rey, McClure, Kavanagh, Cornelissen, et al. 2021). However, in some rare cases, environmental gradients have contributed to a desired fungal morphology and resulted in a substantial increase of the productivities (Bhargava et al. 2003; Bhargava et al. 2003a, b). To evaluate this effect, many studies have focused on quantifying these gradients and addressing the challenges of scale-up. For example, using flow field measurements and computational fluid dynamics (CFD) tools, researchers have confirmed that in a 30 m^3 *Saccharomyces cerevisiae* (*S. cerevisiae*) fermentation, the glucose gradient ranges from 4.3 to 40.7 mg/L (Larsson et al. 1996). In a 12 m^3 *Escherichia coli* (*E. coli*) bioreactor, glucose concentration gradients range from 5 to 35 mg/L, with instantaneous concentrations as high as 2000 mg/L near the feed inlet (Bylund et al. 1998). Similarly, in a 90 m^3 *S. cerevisiae* fermentation, the DO gradient ranges from 0 to 7 mg/L (Nadal-Rey, McClure, Kavanagh, Cassells, et al. 2021), and in a 0.7 m^3 *Streptococcus thermophilic* (*S. thermophilic*) fermentation, pH gradients range from 5.9 to 6.3, with pH levels exceeding 7 near the alkaline solution inlet (Spann et al. 2019). Scale-down studies have shown that when *Aspergillus niger* (*A. niger*) is exposed to substrate gradients, its organic acid by-products including oxalate, citrate, and pyruvate can increase up to twofold (Wang, Liu, et al. 2019). Long-term exposure of *Penicillium chrysogenum* (*P. chrysogenum*) to oxygen-limited conditions may lead to irreversible loss of penicillin production capacity (Vardar and Lilly 1982). In *Corynebacterium glutamicum* (*C. glutamicum*) fermentations, fluctuations in CO_2/HCO_3^- can lead to differential expression of up to 66 genes, with overall changes in gene expression related to the CO_2 gradient range and the cell residence time (Buchholz et al. 2014). While these previous studies have provided valuable insights into the impact of specific environmental gradients on biomass growth and production performance, they do not fully capture the complexity of flow field environments within large-scale bioreactors. For instance, only one single gradient of substrate or DO was simulated in these studies. In reality, DO gradients are inevitably induced with substrate gradients. As a result, incorporating combined environmental gradients into scale-down systems can better simulate microbial metabolic responses under fluctuating conditions at large-scale.

For nearly a century, penicillin has been widely used as a highly effective broad-spectrum antibiotic. Aerobic fed-batch fermentation with *P. chrysogenum* has long been established for commercial production of penicillin and its derivatives. During penicillin production, glucose and DO are the most critical factors affecting process performance. In particular, oxygen, as the terminal electron acceptor in cellular respiration, ensures ATP supply through oxidative phosphorylation (Yang et al. 2022). Furthermore, oxygen is directly involved in the synthesis of isopenicillin N, an intermediate in the penicillin biosynthesis pathway, and its availability is directly correlated with penicillin yield (Janoska et al. 2022). de Jonge et al. (2011) and G. Wang et al. (2018) observed that periodic fluctuations in substrate levels with a cycle time of 360 s led to reduced penicillin productivity by 50% and 65.3%, respectively, possibly due to competition for energy between penicillin biosynthesis and futile cycling of storage carbohydrates. Yang et al. (2022), Janoska et al. (2022), and X. Wang et al. (2024) reported that penicillin production rates are inversely proportional to the duration of oxygen limitation. To evaluate the effect of both glucose and DO gradients in a single study, Janoska et al. (2023) performed combined glucose and DO fluctuation experiments. Their study showed that the decrease in penicillin productivity under combined fluctuations was similar to that observed with only glucose fluctuations, while oxygen fluctuations seldomly affected intracellular metabolite levels. However, in this study, the substrate fluctuations they simulated did not fully capture the transition from substrate excess to substrate limitation, nor did it fully replicate the complex combinatorial gradients of glucose and oxygen typically encountered in industrial-scale bioreactors as proposed by Haringa et al. (2016) and Wei et al. (2023). These factors highlight the challenges of simulating industrial fermentation conditions, and meanwhile underscore the importance of using more sophisticated scale-down models in understanding the dynamic interactions between substrate and DO levels during penicillin production (Kuschel and Takors 2020).

In this study, based on CFD simulation data of an industrial-scale penicillin fermentor by Haringa et al. (2016) and Wei et al. (2023), rational scale-down designs were presented for mimicking both local and global perturbations of substrate and DO gradients. First, two representative local extreme conditions, such as HGLO conditions near the feed inlet and HOLG conditions near the aeration inlet of a 54 m^3 penicillin fermentor were simulated. By doing so, whether the loss of penicillin production capacity in industrial-scale reactors is ascribed to these extreme conditions can be evaluated. Then, the effects of globally combined substrate and DO gradients on metabolic response of *P. chrysogenum* were further explored.

2 | Materials and Methods

2.1 | Materials

The *P. chrysogenum* Wisconsin 54-1255 was purchased from ATCC, fungal spores were prepared on potato dextrose agar (PDA) medium, and the concentrated spore suspensions were stored in aqueous glycerol solution (20% (v/v)) at −80°C. Spore suspension inoculation was used in all experiments and was prepared to ensure that the final spore concentration in the bioreactor after inoculation was about 1×10^6/mL, as described previously.

2.2 | Fermentation Media

The composition of the medium for the batch phase and chemostat cultivation was the same as previously described (X. Wang et al. 2024), containing (g/kg): 16.5 g $C_6H_{12}O_6\,H_2O$, 5 g $(NH_4)_2SO_4$, 1 g KH_2PO_4, 0.5 g $MgSO_4\,7H_2O$, 2 mL trace elements, 1 mL antifoaming agent. The trace element composition (per kg of deionized water) was 75 g $Na_2EDTA\,2H_2O$, 10 g $ZnSO_4\,7H_2O$, 10 g $MnSO_4\,H_2O$, 20 g $FeSO_4\,7H_2O$, 2.5 g $CaCl_2\,2\,H_2O$, 2.5 g $CuSO_4\,5H_2O$. The phenylacetic acid (PAA) concentrations in the batch and the chemostat media were supplied at 0.4085 and 0.68 g/kg, respectively, which was neither limiting nor toxic to cell growth throughout the cultivation (Douma et al. 2012). The preparation and sterilization of the cultivation medium have been described previously (Douma et al. 2010). Briefly, glucose solution and the PAA-containing salt solution were prepared and sterilized at 115 and 121°C for 40 min, respectively. The PAA was dissolved in a KOH solution, with a PAA: KOH molar ratio of 1:1.2 (van Gulik et al. 2000).

2.3 | Experimental Settings

All experiments were performed based on chemostat cultivation systems and independently repeated three times to ensure the reproducibility of the results.

A. Control

   Glucose-limited chemostats with a working volume of 3 L were carried out in a 5 L turbine stirred bioreactor (Shanghai Guoqiang Bioengineering Equipment Co Ltd) at a dilution rate of 0.05 h^{-1}. When the glucose in the batch phase was depleted, the culture was switched to chemostat mode (300 h). The broth was drained by a peristaltic pump through an overflow tube located at the bioreactor gas/liquid interface. The DO level was detected with an oxygen probe (Visiferm DO HAMILTON Switzerland), which was calibrated at 100% at 0.5 bar overpressure (DO approx. 0.4 mM). The temperature was maintained at 25°C, the airflow rate was set at 2 L/min, the stirrer speed was set at 600 rpm and pH was controlled at 6.5 with 4 M sodium hydroxide using a sterilizable pH probe (Mettler-Toledo, Greifensee, Switzerland). The off-gas oxygen and carbon dioxide fractions were monitored in real-time using an off-gas mass spectroBhargavameter (Prima BT, Thermo Fisher Scientific Winsford U.K.CW7 3GA). Samples for measuring CDW, products, and by-products were collected every 12 h during the chemostat phase. After 100 h of the chemostat phase, samples for metabolomics analysis were collected every 24 h.

B. Experimental Setup I: High-Glucose Low-Oxygen (HGLO)

   After the batch fermentation, a continuous culture of 300 h was initiated, which can be divided into three typical stages: Steady state phase (0–100 h), the experimental phase (100–200 h), and the recovery phase (200–300 h). The steady state and recovery phases followed the same conditions as the control. During the experimental phase, glucose solution was fed in a pulse-pause manner during the first 15 s of each 150-second cycle at a rate 10 times higher than the control, followed by 135 s without feeding to maintain an average glucose feed rate equal to that of the control with a continuous feeding mode. Oxygen partial pressure in the inlet gas was maintained at approximately 1%, with three mass flow controllers regulating gas flow (Figure 1A). Samples were collected every 12 h during the continuous culture phase for measuring cell dry weight (CDW), products, and by-products. After the steady state phase, metabolomics samples were collected every 24 h (between 22 and 24 s of the cycle). During the last cycle of the experimental phase, samples were collected every 15 s to verify substrate concentration fluctuations.

C. Experimental Setup II: High-Oxygen Low-Glucose (HOLG)

   During the experimental phase, the oxygen partial pressure in the inlet gas was maintained at approximately 17.5%, while all other conditions were identical to those in Experimental Setup I (Figure 1A). After the steady state phase, metabolomics samples were collected every 24 h (between 140 and 150 s of the cycle). During the last cycle of the experimental phase, samples were collected every 15 s to verify substrate concentration fluctuations.

D. Experimental Setup III: Global Fluctuations in Glucose and Oxygen (GFGO)

   During the experimental phase, pulse-pause feeding was implemented with a 360-second cycle: glucose was fed during the first 36 s at a rate 10 times higher than the control, followed by 324 s without feeding. The specific operation followed the protocol of de Jonge et al. (2011). High-purity air was introduced for 210 s starting at the 75-second mark, followed by high-purity nitrogen for 150 s (Figure 1B). After the steady state phase, metabolomics samples were collected every 24 h (at 270 s of the cycle). During the experimental period, a series of samples for detecting the concentration changes of both intracellular and extracellular metabolites were collected as follows for the last two cycles: 0 s, 8 s, 16 s, 26 s, 36 s, 50 s, 70 s, 90 s, 110 s, 145 s, 180 s, 200 s, 220 s, 240 s, 260 s, 280 s, 320 s, and 350 s.

2.4 | Cell Dry Weight

CDW was measured by weight difference between empty glass fiber filters (47 mm in diameter, 0.8-μm pore size, type A/E; Pall Corporation, East Hills, NY, USA) and dry glass fiber filters with biomass. About 15 mL of broth was withdrawn and divided into three portions for CDW measurements. For each CDW sample, 5 mL of the broth was filtered, and the cell cake was washed three times with 10 mL of demineralized water and dried in a microwave oven (power 800 W) for 6 min. The filter containing biomass was cooled to room temperature in a desiccator and weighed.

2.5 | Rapid Sampling, Quenching, and Metabolite Extraction

For extracellular sampling, the cold steel-bead method combined with liquid nitrogen was used for the fast filtration and quenching

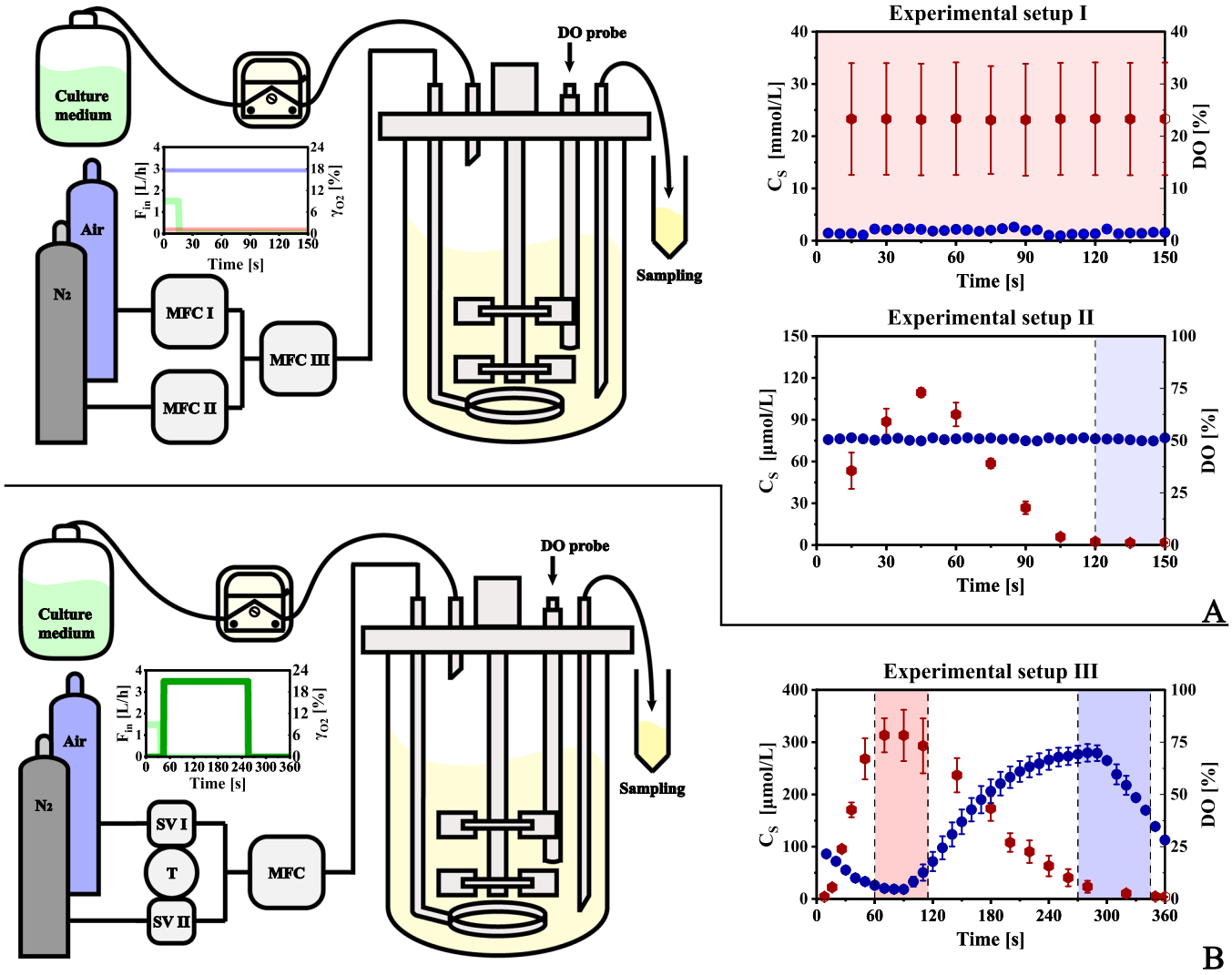

FIGURE 1 | Experimental setup and completion status. (A) HGLO and HOLG. (B) GFGO. represents partial pressure of oxygen in HGLO. represents partial pressure of oxygen in HOLG. represents partial pressure of oxygen in GFGO. represents feeding flow rate during experimental phase. • represents extracellular sugar concentration. • represents dissolved oxygen level. Red rectangle corresponds to HGLO. Blue rectangle corresponds to HOLG. All error bars represent the standard deviation of data obtained from three independent biological replicates.

of extracellular enzyme activities, as described previously (Wang, Chu, et al. 2019). For intracellular sampling, approximately 1.3 mL of broth was taken from the bioreactor into a tube containing the quenching solution (−27.5°C, 40% V/V aqueous methanol). A customized rapid sampling device was developed to ensure fast sampling and rapid quenching, avoiding as much as possible changes in intracellular metabolites. For detailed sampling procedures, please refer to Li et al. (2018). A rapid filtration and cold washing method was used to quickly and efficiently remove all compounds present outside the cells. In this study, a previously well-established protocol for rapid sampling, quenching, and subsequent metabolite extraction was followed, as previously described (Wang, Chu, et al. 2019). For quantification of intracellular metabolites, isotope dilution mass spectrometry (IDMS) method was used to correct most aspects of analytical bias (Mashego et al. 2005). To achieve this, U-^{13}C-labeled cell extracts obtained from *Pichia pastoris* fed-batch cultures were added as internal standards in the sample before intracellular metabolite extraction (Wu et al. 2005).

2.6 | Analytical Methods

Quantification of intracellular amino acids, sugar phosphates, organic acids, and sugar alcohols was performed by gas chromatography-mass spectrometry (GC-MS) (7890A GC coupled to 5975C MSD; Agilent Technologies, Santa Clara, CA, USA). The analytical procedures were performed according to de Jonge et al. (2014), with slight modifications in the column and temperature gradients. For specific settings, please refer to X. Liu et al. (2019).

An Agilent Zorbax SB-C_{18} reversed-phase column (150 mm × 4.6 mm ID, 5 μm) was used to determine the concentrations of PAA, penicillin G, and byproducts in the penicillin biosynthetic pathway using an isocratic reversed-phase high-performance liquid chromatography (HPLC) method. The mobile phase was 0.44 g/L potassium dihydrogen phosphate in acetonitrile/water (65/35, v/v); the injection volume was 5 μL, the detection wavelength was 214 nm, the flow rate was 1.5 mL/min and the column temperature was 25°C (X. Wang et al. 2024).

2.7 | Cytosolic Free NADH/NAD$^+$ Ratio

The cytosolic free NADH/NAD$^+$ ratio was calculated using an equilibrium pool of C_4 (aspartate and malate) pool in the tricarboxylic acid cycle (TCA) cycle under the assumption of constant K′ and intracellular pH (Nasution et al. 2006):

$$\frac{\text{NADH}}{\text{NAD}^+} = \text{K}'\frac{\text{Malate*Glutamate}}{\alpha KG\text{*Aspartate*H}^+}$$

2.8 | Flux Balance Analysis

The genome-scale metabolic model (GEM) of *P. chrysogenum* was utilized for the estimation of metabolic flux distribution in this study. The linear programming solver Gurobi 5 (v9.5.1) was employed to solve the model with the maximum growth set as the objective function (X. Wang et al. 2024).

2.9 | Orthogonal Partial Least Squares Discriminant Analysis (OPLS-DA)

OPLS-DA was performed using MetaboAnalyst 5.0 (https://new.metaboanalyst.ca/home.xhtml). Based on the targeted metabolomics data from each experimental setup against the corresponding control data, the top 30 metabolites with the highest Variable Importance in Projection (VIP) scores were extracted.

3 | Results and Discussion

3.1 | Local and Global Heterogeneous Environments Simulation: HGLO and HOLG Conditions

As previously reported by Haringa et al. (2016), CFD simulations with glucose uptake kinetics predict that the glucose concentration gradient in a 54 m^3 penicillin bioreactor with *P. chrysogenum* spans ten orders of magnitude, ranging from 10^{-7} to 10^3 μmol/kg. Based on the relation between substrate concentration (C_S) and the substrate affinity constant (K_S), the entire gradient can be divided into three representative regions: the substrate-excess zone ($C_S > 19K_S$), the substrate-limited zone ($1/19\ K_S < C_S < 19K_S$), and the substrate-starved zone ($C_S < 1/19\ K_S$). Wei et al. (2023) extended the simulations to include mixed glucose-oxygen limitation, predicting an oxygen-limited zone with a DO concentration below 0.05 mM above the top impeller in the same 54 m^3 penicillin bioreactor. Based on this, two local extreme conditions at comparable large-scale were scaled-down at laboratory-scale: the feed inlet region near the top of the reactor (HGLO zone) and the aeration inlet region near the bottom (HOLG zone). These two regions are expected to correspond to the substrate-excess, oxygen-limited zone predicted near the glucose feed, and the substrate-starved, oxygen-sufficient zone predicted near the sparger, respectively. Based on the experimentally determined substrate affinity constant of *P. chrysogenum* in this study, the target conditions for the HGLO setting were defined as $C_S > 296.97$ μM and DO < 0.05 mM, while for the HOLG setting, the target conditions were defined as $C_S < 0.8$ μM and DO > 0.05 mM. To further investigate the effects of combined substrate and DO gradients on penicillin production and the metabolism of *P. chrysogenum*, global fluctuations in glucose and oxygen (GFGO) was designed to simulate combined fluctuations. As previously described, cells circulating throughout the 54 m^3 bioreactor are expected to experience fluctuations in substrate concentrations ranging from starvation to excess, coupled with corresponding fluctuations in DO concentrations from oxygen-sufficient to oxygen-limited conditions. Therefore, the target design for the combined fluctuation experiment involved a 360-second cyclic fluctuation of substrate and DO concentrations, alternating between periods of HGLO ($C_S > 296.97$ μM, DO < 0.05 mM) and HOLG ($C_S < 0.8$ μM, DO > 0.05 mM) environments for a defined duration.

Under HGLO conditions, the substrate concentration remained consistently above 20 mM, while the DO concentration was maintained below 3% (0.012 mM) throughout the experiment (Figure 1A). This fully meets the target HGLO conditions for the entire 150-second cycle, corresponding to the environment around the feed inlet as predicted by the CFD model. Under HOLG conditions, the substrate concentration fluctuated periodically, dropping below 0.8 μM between the 120th and 150th seconds of the cycle, while the DO concentration remained stable around 50% (0.2 mM) throughout the experiment (Figure 1A). As a result, the target HOLG conditions were met during the last 30 s of each 150-second cycle, corresponding to the environment around the aeration inlet. Since the substrate concentration during the HOLG cycle did not exceed 296.97 μM, the entire cycle can be considered representative of cells circulating in the region below the top impeller of the 54 m^3 bioreactor. According to the experimental results in this study (Figure 1B), the concentrations of substrate (ranging from 3.8 to 313.1 μM) and DO (ranging from 4.7% to 74.2%; 0.019 μM to 0.297 mM) fluctuated alternately throughout the cycle. The HGLO scenario occurred at the 60-second mark and lasted for approximately 45 s, while the HOLG scenario occurred at the 270-second mark and lasted for 75 s. Overall, these simulated combined fluctuations in our scale-down systems align well with the range of substrate and DO fluctuations that cells would experience while circulating through the entire 54 m^3 bioreactor.

3.2 | More Pronounced Metabolic Impact Under HGLO Conditions

Under HGLO conditions, the biomass concentration of *P. chrysogenum* decreased by approximately 42.1% compared to the control group (Figure 2A, Supporting Information S1: Figure 1). This phenomenon was not observed in the low-oxygen chemostat experiment previously performed by Yang et al. (2022), where the DO concentration was maintained at 5%. This may be because a DO concentration of 5% (0.15 mM) did not fall below the threshold necessary for cellular growth. According to Janoska et al. (2023), the critical oxygen concentration for *P. chrysogenum* growth is 0.13 mM, whereas in this study, the DO concentration under HGLO conditions was even lower, around 3% (0.012 mM). The consumption of the precursor PAA

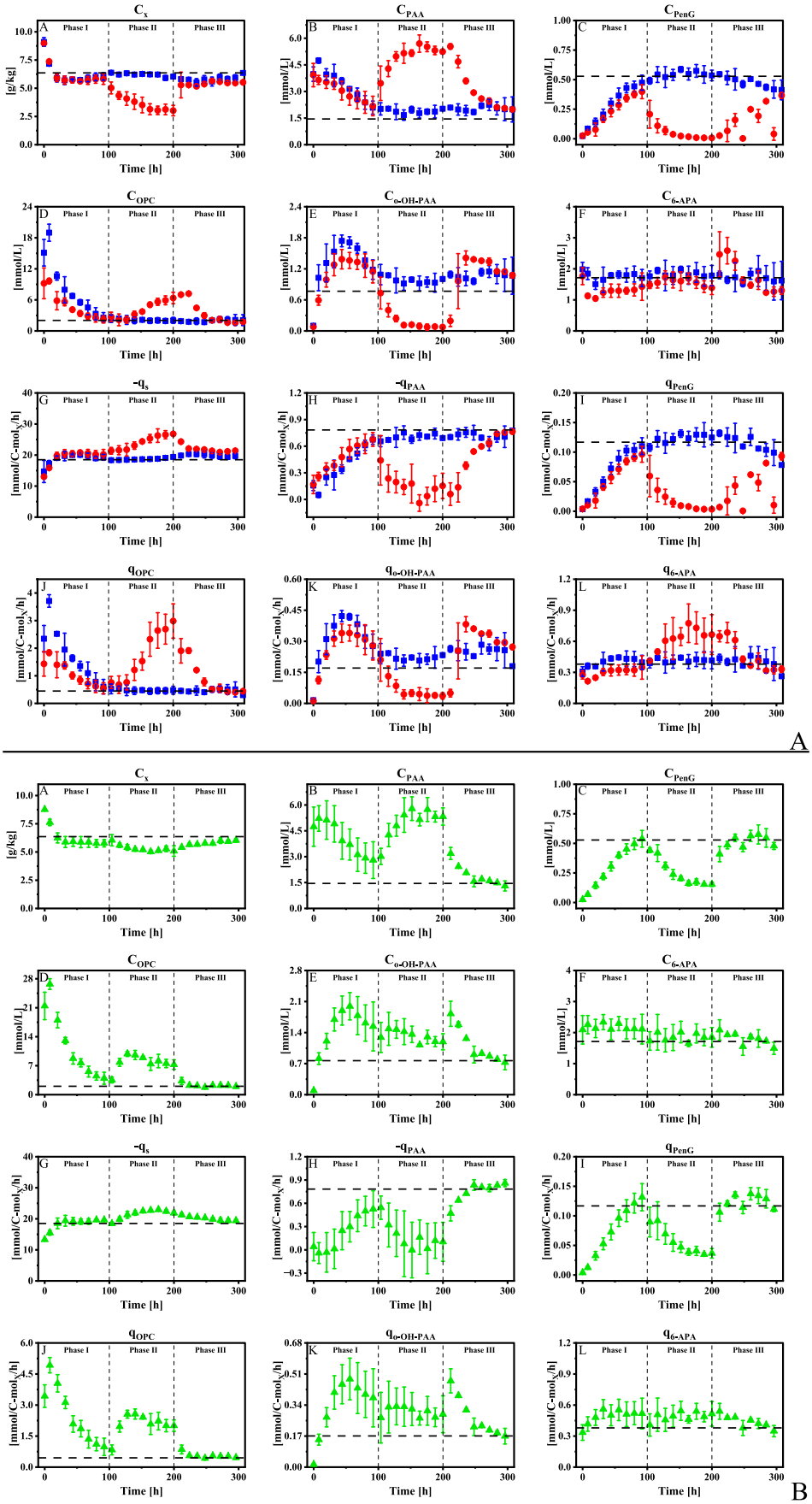

FIGURE 2 | Legend on next page.

approached zero, with the specific consumption rate decreasing by approximately 79.3%. Correspondingly, penicillin production and productivity also gradually decreased to near zero during the HGLO phase. This seems reasonable that oxygen, as one of the substrates, is directly involved in the biosynthesis of isopenicillin N (Janoska et al. 2022). Under extreme low-oxygen conditions, the reduced supply of the direct precursor isopenicillin N likely contributed to the decline in penicillin production. Meanwhile, the consumption of the side-chain precursor PAA was significantly reduced (Bainbridge et al. 2007; White et al. 1982). Additionally, the high extracellular glucose concentration may have induced substrate inhibition, further contributing to the reduction in penicillin productivity (Revilla et al. 1986).

Meanwhile, it is apparent that the accumulation of the by-product 6-oxopiperidine-2-carboxylic acid (OPC) under HGLO conditions was twice that of the control, with its specific production rate increasing by approximately 2.6-fold (Figure 2A, Supporting Information S1: Figure 1). The levels of 2-hydroxyphenylacetic acid (*o*-OH-PAA) and its specific production rate, however, approached zero. This is likely due to the limited availability of oxygen, as the enzyme phenylacetate hydroxylase, which catalyzes the conversion of PAA to *o*-OH-PAA, requires oxygen for its activity (Deshmukh et al. 2015). In our recent study, we also observed that PAA was barely converted into *o*-OH-PAA and thus its recovery is nearly closed under periodic fluctuations in DO concentrations (X. Wang et al. 2024). Interestingly, the level of 6-aminopenicillanic acid (6APA) decreased by approximately 8.84% compared to the control, while its specific production rate increased by approximately 38.7%. According to documented pathways, 6APA is only formed through the degradation of penicillin or isopenicillin (Deshmukh et al. 2015). However, under HGLO conditions, there is clearly insufficient precursor to maintain its content. Hence, it is hypothesized that there may be unknown pathways contributing to its production, independent of secondary metabolism related to penicillin production.

During the recovery phase of HGLO conditions, biomass concentration remained approximately 14.7% lower than that of the control. Although penicillin production and productivity were gradually increased, they did not fully recover. This finding is similar to a previous report by Vardar and Lilly (1982), which indicated that prolonged exposure of *P. chrysogenum* to oxygen-limited conditions at or below the critical oxygen concentration could result in irreversible damage to its production capacity. At the end of the recovery phase, the concentrations of PAA and other by-products, along with their specific consumption/production rates, were gradually restored and approached those of the control.

Under HOLG conditions, nearly all measured parameters, including biomass, precursors, products, and by-products, as well as their specific consumption/production rates, showed no significant difference compared to the control, with fluctuations of no more than 10%. However, a decline in biomass concentration was observed during the recovery phase of HOLG, which did not occur under control conditions. During this period, biomass concentration was approximately 9.3% lower than that of the control. As shown in Figure 2A, extracellular penicillin concentration gradually decreased, with its specific production rate dropping by an average of 0.67% every 12 h. This premature degeneration phenomenon was not observed either under control or under HGLO conditions. The extracellular concentration and specific production rate of the by-product *o*-OH-PAA increased gradually during the recovery phase. According to the literature, PAA enters the cell via passive transport (Douma et al. 2012), and this compound is toxic to the cell. One of the primary detoxification mechanisms of *P. chrysogenum* involves hydroxylating PAA to form *o*-OH-PAA, which is then excreted extracellularly or degrading it via the gentisate pathway to enter the TCA cycle. Another mechanism involves activating PAA as a side-chain precursor for the biosynthesis of penicillin G, which is subsequently excreted extracellularly (Jami et al. 2010). Therefore, the increased extracellular levels of *o*-OH-PAA may be related to the gradual decline in penicillin production during this process.

According to Table 1, it is evident that the HGLO environment has a greater impact on the physiological state of *P. chrysogenum* than the HOLG environment. Specifically, under HGLO conditions, there is a noticeable reduction in specific formation rates of carbon dioxide, penicillin as well as the associated by-products compared to the control. However, there is a noticeable increase in the rate of substrate consumption under HGLO phase. Collectively, the results suggest an increased excretion of intracellular metabolites and/or enhanced accumulation of intracellular storage carbohydrates.

Under GFGO conditions, the biomass yield decreased significantly by approximately 16.2% compared to the control (Figure 2B, Supporting Information S1: Figure 1). Similar findings were observed in our previous studies where we investigated periodic single substrate fluctuations with a 360-second cycle (G. Wang et al. 2018), and periodic single DO fluctuations with a 150-second cycle (0.015–0.135 mM) (X. Wang et al. 2024). However, this result differs from the study by Janoska et al. (2023), where no growth impact was observed under GFGO conditions with a 360-second cycle. This discrepancy is likely due to the design limitations of the study of Janoska et al. (2023), where the substrate fluctuations did not reach excess concentrations, nor did they induce substrate starvation conditions.

Interestingly, the biomass concentration at the first sampling point during the experimental phase under the GFGO conditions showed a 4.7% increase compared to pre-switch conditions, suggesting a shift from secondary metabolism to primary metabolism. Consistent with this, Yang et al. (2022) observed

FIGURE 2 | Concentration and biomass-specific rates of metabolites related to penicillin biosynthesis. ▬ ▬ ▬ represents the mean value of the control. (A) HGLO and HOLG; (B) GFGO. ● represents the mean value of HGLO. ■ represents the mean value of HOLG. ▲ represents the mean value of GFGO. Phase I (0–100 h), II (100–200 h), and III (200–300 h) correspond to steady state, experimental, and recovery phase, respectively. All error bars represent the standard deviation of data obtained from three independent biological replicates.

TABLE 1 | Biomass-specific rates and yields under HGLO and HOLG conditions.

			HGLO		HOLG	
Parameters	**Units**	**Control**	**Experimental phase**	**Recovery phase**	**Experimental phase**	**Recovery phase**
$-q_S$	mmol/C-mol$_X$/h	18.31 ± 0.20	24.12 ± 0.61*	21.54 ± 0.096*	18.73 ± 0.05*	20.05 ± 0.46
$-q_{O_2}$	mmol/C-mol$_X$/h	80.40 ± 0.77	48.74 ± 2.95**	95.66 ± 0.22**	87.83 ± 2.99	88.85 ± 3.51
q_{CO_2}	mmol/C-mol$_X$/h	83.93 ± 0.44	55.69 ± 1.18***	96.74 ± 0.70*	90.04 ± 1.32*	91.55 ± 2.89
$-q_{PAA}$	mmol/C-mol$_X$/h	0.78 ± 0.017	0.16 ± 0.056**	0.51 ± 0.017*	0.70 ± 0.020	0.71 ± 0.012*
q_{PenG}	mmol/C-mol$_X$/h	0.12 ± 0.0063	0.018 ± 0.0051***	0.04 ± 0.0002***	0.12 ± 0.0041	0.12 ± 0.0079
q_{OPC}	mmol/C-mol$_X$/h	0.45 ± 0.097	1.73 ± 0.22*	0.90 ± 0.087	0.48 ± 0.072	0.47 ± 0.056
$q_{o-OH-PAA}$	mmol/C-mol$_X$/h	0.17 ± 0.0062	0.075 ± 0.020*	0.29 ± 0.011	0.22 ± 0.012	0.26 ± 0.018*
q_{6APA}	mmol/C-mol$_X$/h	0.38 ± 0.0062	0.62 ± 0.072	0.46 ± 0.0024*	0.41 ± 0.031	0.42 ± 0.035
C_X	g/kg	6.36 ± 0.060	3.68 ± 0.28*	5.42 ± 0.095	6.29 ± 0.016**	5.77 ± 0.15
OUR	mmol/L/h	18.10 ± 0.044	6.43 ± 0.791	18.49 ± 0.366	19.404 ± 0.680	18.24 ± 0.516
CER	mmol/L/h	18.90 ± 0.128	7.29 ± 0.499	18.70 ± 0.463	19.89 ± 0.307	18.79 ± 0.152
RQ	—	1.04 ± 0.0045	1.15 ± 0.063	1.01 ± 0.0050	1.03 ± 0.020	1.03 ± 0.022
$Y_{X/S}$	Cmol/Cmol	0.46 ± 0.0049	0.35 ± 0.0088**	0.39 ± 0.0017*	0.44 ± 0.0011*	0.42 ± 0.0095
$Y_{P/S}$	μCmol/Cmol	17.00 ± 0.78	2.02 ± 0.60***	5.00 ± 0.051***	17.49 ± 0.56	15.94 ± 0.69
$Y_{CO_2/S}$	Cmol/Cmol	0.76 ± 0.010	0.39 ± 0.0060****	0.75 ± 0.0088	0.80 ± 0.0098	0.76 ± 0.011

Note: Two two-tailed *t*-test was conducted using SPSS 25. $p < 0.05$ indicates significant difference (*). $p < 0.01$ indicates a highly significant difference (**). $p < 0.005$ (***). $p < 0.001$ (****).

TABLE 2 | Biomass-specific rates and yields under GFGO conditions.

Parameters	Units	Control	GFGO	
			Experimental phase	Recovery phase
$-q_S$	mmol/Cmol$_X$/h	18.31 ± 0.20	21.41 ± 0.40	19.96 ± 0.35
$-q_{PAA}$	mmol/Cmol$_X$/h	0.78 ± 0.017	0.17 ± 0.16	0.75 ± 0.0037
q_{PenG}	mmol/Cmol$_X$/h	0.12 ± 0.0063	0.056 ± 0.0076*	0.12 ± 0.0052
q_{OPC}	mmol/Cmol$_X$/h	0.45 ± 0.097	2.07 ± 0.11**	0.55 ± 0.01
$q_{o-OH-PAA}$	mmol/Cmol$_X$/h	0.17 ± 0.0062	0.30 ± 0.054	0.27 ± 0.0047*
q_{6-APA}	mmol/Cmol$_X$/h	0.38 ± 0.0062	0.49 ± 0.051	0.444 ± 0.00045**
C_X	g/kg	6.36 ± 0.060	5.33 ± 0.071**	5.78 ± 0.085
$Y_{X/S}$	Cmol/Cmol	0.46 ± 0.0049	0.39 ± 0.0073	0.42 ± 0.0074
$Y_{P/S}$	μCmol/Cmol	17.00 ± 0.78	6.07 ± 0.53*	16.51 ± 0.98

Note: Two-tailed *t*-test was conducted using SPSS 25. $p < 0.05$ indicates a significant difference (*). $p < 0.01$ indicates a highly significant difference (**). $p < 0.005$ (***). $p < 0.001$ (****).

this increase in a 5% (0.015 mM) low-oxygen stress experiment, and Janoska et al. (2022) observed a similar response in their 120-second periodic single DO fluctuation study (0–0.127/0.178 mM). The extracellular concentration of the PAA under GFGO conditions was approximately 2.6 times higher than that of the control, and its specific consumption rate decreased by about 77.9%. The extracellular concentration of penicillin decreased by about 63.9%, with production capacity reduced by 53.3%. This reduction lies between the results observed in the HGLO and HOLG conditions (Table 2), which aligns with other studies on single substrate or DO fluctuations (de Jonge et al. 2011; Janoska et al. 2023; Janoska et al. 2022; G. Wang et al. 2018).

The accumulation of the by-product OPC exceeded that of the control by more than threefold, with its specific production rate increasing by approximately 3.6 times. The accumulation was higher than that observed under HGLO conditions, and the accumulation pattern differed from that observed under those conditions (Figure 2A). This larger accumulation may be related to the intracellular levels of the precursor α-aminoadipate acid. Since OPC production is an enzymatic process (Henriksen et al. 1998), differences in accumulation trends may be attributed to variations in enzyme levels or activity under different conditions. Similarly, the accumulation of *o*-OH-PAA increased by approximately 23.9%, with its specific production rate increasing by about 76.5% compared to the control. This is likely because, as cells shift from secondary to primary metabolism, the gentisate pathway is activated to degrade PAA, and the conversion of PAA to *o*-OH-PAA is the first step in this process (Jami et al. 2010). The relatively stable production of 6APA under GFGO conditions was similar to that observed under HOLG conditions (Figure 2A).

During the recovery phase of GFGO conditions, biomass yield increased but remained approximately 9.1% lower than the control. The specific consumption rate of PAA and the specific production rate of penicillin returned to levels similar to the control (Table 2). This contrasts with the recovery phase observed in HGLO (Table 1), suggesting that the duration of exposure to oxygen levels below the critical concentration plays a critical role (150 s per cycle in HGLO vs. 45 s per cycle in GFGO). Consistent with this, Vardar and Lilly (1982) previously reported that prolonged fluctuations around the critical oxygen concentration or long-term hypoxia could lead to irreversible reductions in penicillin production. Based on the fact that no significant impact was observed under HOLG conditions (Table 1), it can be inferred that short-term, single substrate fluctuations do not cause irreversible damage to penicillin production. However, large substrate gradients are one of the major factors leading to the observed production performance loss.

3.3 | Metabolic Responses of *Penicillium chrysogenum* to Local and Global Heterogeneous Environments

3.3.1 | Overall Observations

OPLS-DA was performed using the targeted metabolomics data from both the HGLO and HOLG conditions, as compared with that of the control group (Figure 3A,B). Consistently, the results indicated that HGLO conditions induced more significant metabolic shifts than HOLG conditions at the metabolite level. The VIP scores showed that among the top 10 marker metabolites, half of them in the HGLO-control comparison were amino acids, whereas only two were observed in the HOLG-control comparison. Under HOLG conditions, more differential metabolites were localized within the Embden–Meyerhof–Parnas (EMP) pathway and storage metabolism.

The OPLS-DA analysis revealed significant group differences between the combined fluctuation at the 270-second point and the control condition, although the sampling during fluctuation also led to substantial within-group variation (Figure 3C). The VIP score chart showed that amino acids accounted for approximately 73% of the marker metabolites with scores above 1, a higher proportion than in the HGLO and HOLG conditions (Figure 3A,B). Taken together, the results suggest that the cells may have adopted different metabolic strategies to cope with local and global substrate and DO gradients.

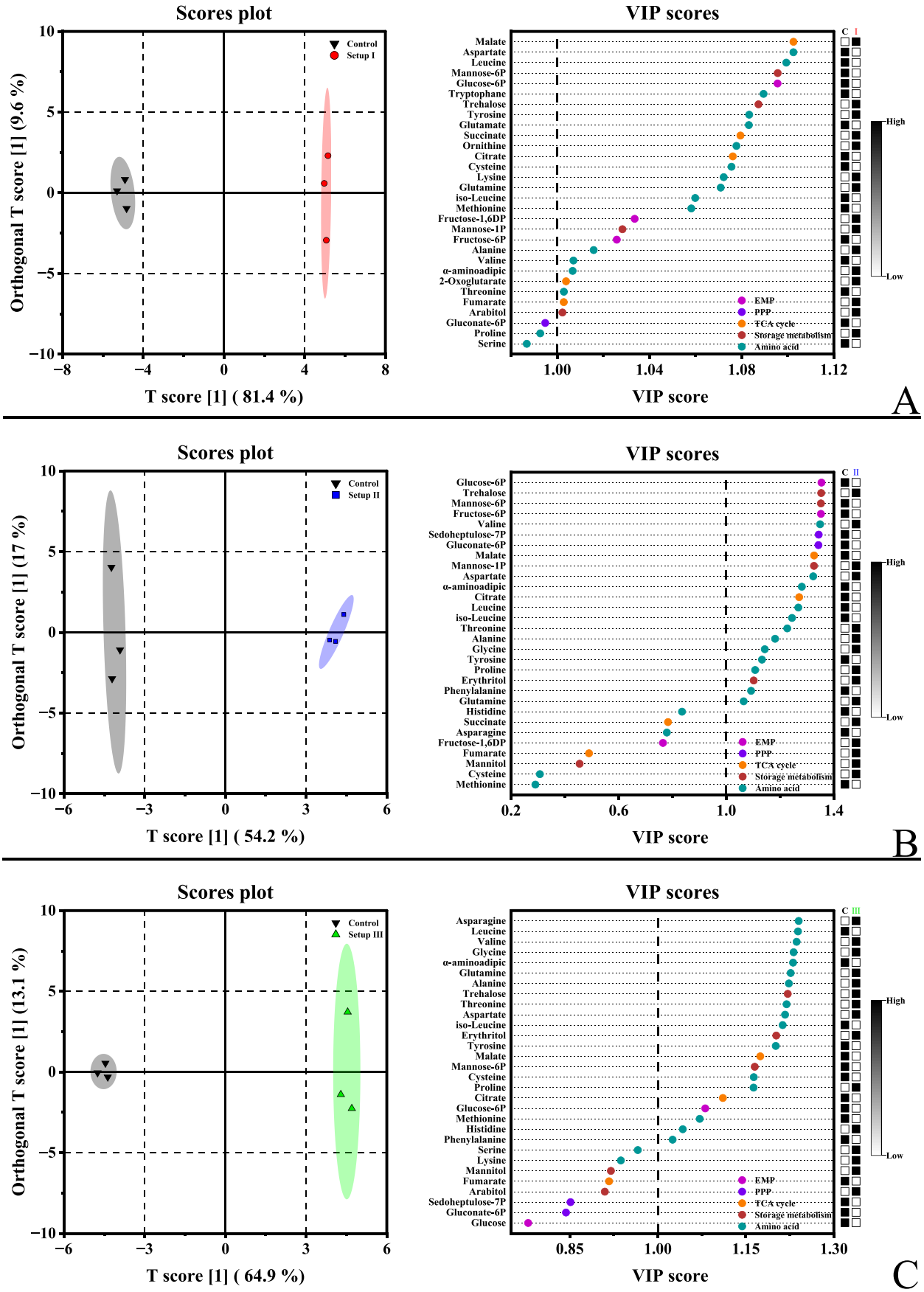

FIGURE 3 | The results of orthogonal partial least-squares discriminant analysis (OPLS-DA). Quantitative metabolomic data from each experimental setup were analyzed using separate OPLS-DA comparisons against the control data. (A) HGLO; (B) HOLG; (C) GFGO. Group A: R2Y = 0.999, Q2 = 0.987, $p = 0.0975$; Group B: R2Y = 0.998, Q2 = 0.951, $p = 0.0975$; Group C: R2Y = 0.999, Q2 = 0.961, $p = 0.097$.

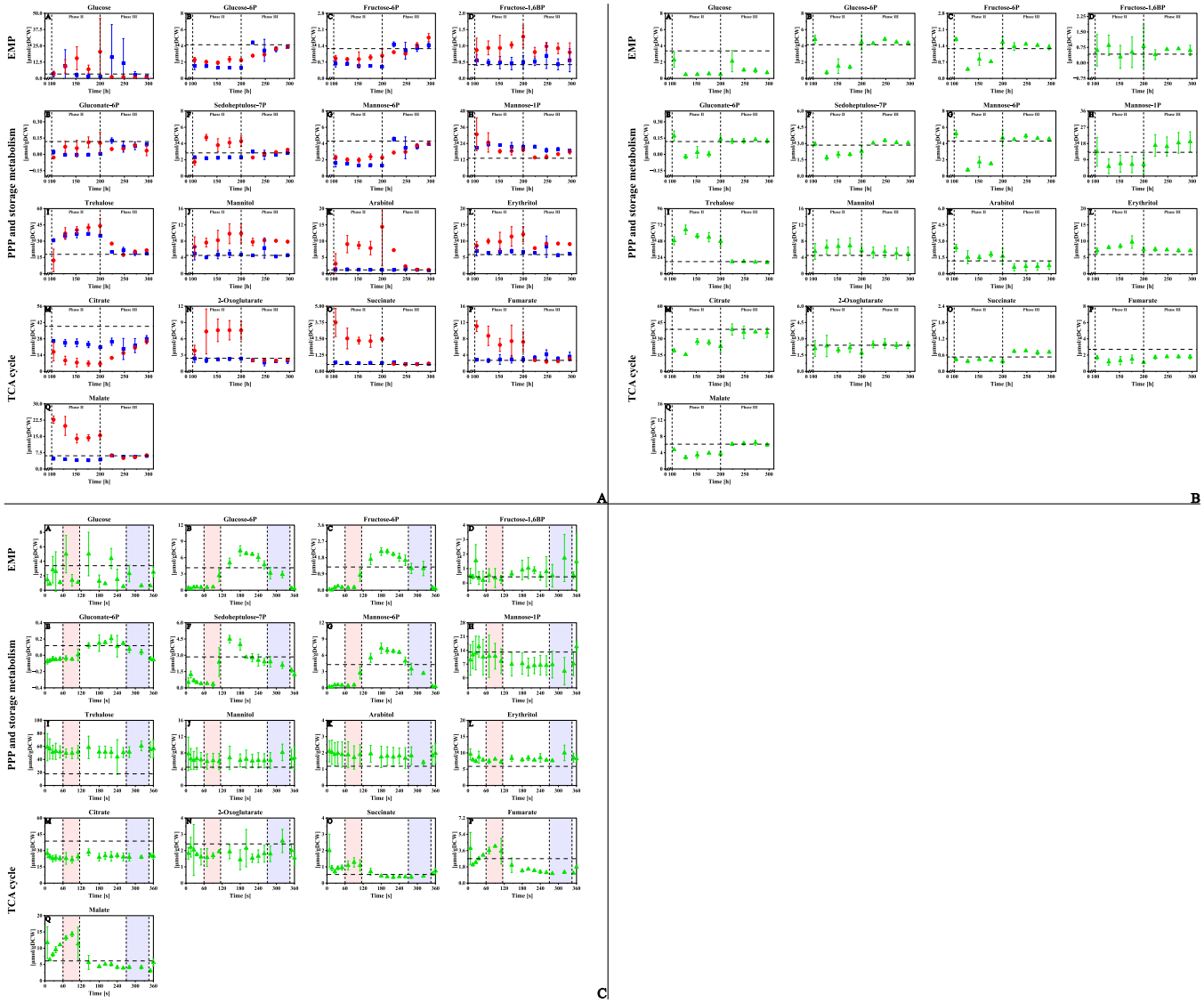

FIGURE 4 | Intracellular amounts of central carbon metabolites. (A) HGLO and HOLG; (B) GFGO long term; (C) GFGO single cycle. ▬ ▬ ▬ represents the mean value of the control. ● represents the mean value of HGLO. ■ represents the mean value of HOLG. ▲ represents the mean value of experimental setup III. Phases I, II, and III correspond to steady state, experimental, and recovery phase, respectively. Red rectangular area corresponds to HGLO. Blue rectangular area corresponds to HOLG. All error bars represent the standard deviation of data obtained from three independent biological replicates.

3.3.2 | Central Carbon Metabolism

Under HGLO conditions, the intracellular glucose concentration increased continuously with time, reaching 20.5 μmol/gDCW (Figure 4A). This suggests that the cells were adapting to the high extracellular glucose concentration. As shown in Figure 4A and Supporting Information S1: Figure 2, the intracellular levels of glucose-6-phosphate (G6P) and fructose-6-phosphate (F6P) in the glycolysis pathway decreased by approximately 47.8% and 31.3%, respectively. In the pentose phosphate (PP) pathway, the level of 6-phosphogluconate (6PG) initially decreased before recovering, while sedoheptulose-7-phosphate (S7P) increased by about 31.3%. This suggests that central carbon metabolism tends to favor the PP pathway under these conditions. The storage metabolites mannose-6-phosphate (M6P) and mannose-1-phosphate (M1P) showed opposite trends: M6P decreased by about 49.2%, while M1P increased by 70%, and mannitol levels increased by approximately 87.6%. It has been documented that converting mannitol to M6P requires cytochrome c (Arcus and Edson 1956), which is disrupted under low-oxygen conditions, thereby blocking the conversion of mannitol to M6P. The intracellular levels of trehalose, arabitol, and erythritol increased by 97.1%, 632%, and 77.0%, respectively. In the TCA cycle, the levels of α-ketoglutarate, succinate, fumarate, and malate increased by two to three times. This is likely due to the impaired electron transport chain under low-oxygen conditions, resulting in an accumulation of the TCA cycle intermediates. The intracellular levels of organic acids produced via the glyoxylate shunt also increased significantly, suggesting that the cells activated this pathway to reduce the production of reducing power and maintain redox balance under low-oxygen conditions (Holmes et al. 1991; Mu et al. 2021). This is consistent with our previous finding where flux balance analysis also suggested a significant upregulation of the glyoxylate shunt under low-oxygen stress (Yang et al. 2022). By the end of the recovery phase, only G6P, M6P,

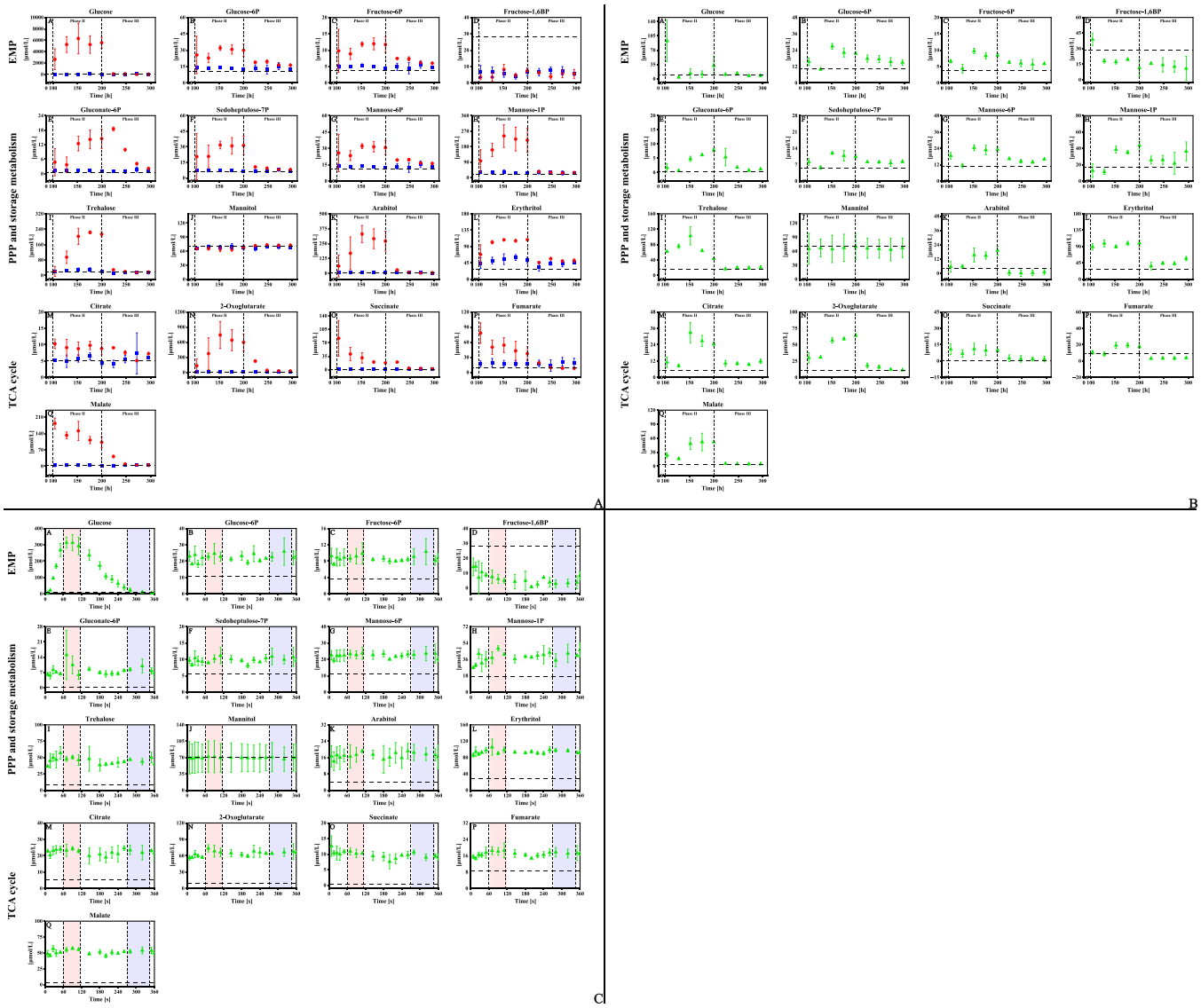

FIGURE 5 | Extracellular concentration of central carbon metabolites. (A) HGLO and HOLG; (B) GFGO long term; (C) GFGO single cycle. ▬ ▬ ▬ represents the mean value of the control. ● represents the mean value of HGLO. ■ represents the mean value of HOLG. ▲ represents the mean value of GFGO. Phases I, II, and III correspond to steady state, experimental, and recovery phases, respectively. Red rectangular area corresponds to HGLO. Blue rectangular area corresponds to HOLG. All error bars represent the standard deviation of data obtained from three independent biological replicates.

α-ketoglutarate, succinate, fumarate, and malate returned to levels comparable to the control.

Fructose-1,6-bisphosphate (FBP) tended to accumulate intracellularly under HGLO conditions, with its extracellular concentration decreasing by approximately 80.6% compared to the control (Figure 5A, Supporting Information S1: Figure 3), while its intracellular concentration increased by about 2.4 times. Previous studies have shown that *Escherichia coli* cells activated the methylglyoxal pathway (a low-energy-generating bypass of the EMP pathway) during substrate fluctuations by adjusting the flux through the FBP branch point towards dihydroxyacetone phosphate and glyceraldehyde-3-phosphate (Weber et al. 2005). The extracellular concentration of mannitol remained consistent with that of the control. Except for these two metabolites, the extracellular levels of other central carbon metabolites increased significantly (Figure 5A, Supporting Information S1: Figure 3), consistent with an increased gap in the carbon recovery described in Section 3.2. Severe oxygen limitations under HGLO conditions led to insufficient electron acceptors for the electron transport chain. Due to limited ATP supply under such conditions, the cells likely enhanced glucose uptake rate (Table 1), which is speculated to be involved in generating ATP via substrate-level phosphorylation and at the same time excretes metabolites to make it more feasible. Notably, the extracellular concentration of α-ketoglutarate increased by approximately 50 times compared to the control (Figure 5A, Supporting Information S1: Figure 3), contrasting with the changes in the extracellular concentrations of succinate, fumarate, and malate downstream of the glyoxylate pathway. This indicates that the major reducing power producing steps in the TCA cycle were severely impaired. Moreover, under low-oxygen conditions, cells tend to upregulate α-ketoglutarate biosynthesis to ensure efficient ammonium

assimilation, further contributing to the intracellular and extracellular accumulation of α-ketoglutarate (Z. Liu and Butow 2006).

Under HOLG conditions, intracellular glucose levels initially increased and then decreased to levels similar to those in the control (Figure 4A, Supporting Information S1: Figure 2), indicating an adaptation to external glucose perturbations. The reductions in G6P and F6P in the glycolysis pathway were approximately 20% greater under HOLG than under HGLO conditions. In the PP pathway, 6PG levels tended toward zero, and S7P levels slightly decreased. The levels of M1P and trehalose increased by approximately 60.5% and 94.6%, respectively, compared to the control, indicating that more carbon was directed into storage metabolism. de Jonge et al. (2014) also reported that trehalose cycling is essential for *P. chrysogenum* to cope with fluctuating substrate environments. Although trehalose synthesis and degradation consume extra energy, the stored trehalose provides a carbon and energy reserve for cells during substrate starvation, buffering against environmental fluctuations. In the TCA cycle, the intracellular level of citrate decreased by about 38.7%, similar to the trend under HGLO conditions, while the levels of other organic acids showed no significant differences compared to the control (Figure 4A, Supporting Information S1: Figure 2). Notably, the intracellular concentration of citrate decreased under both conditions in this study, consistent with findings from G. Wang et al. (2018) and Yang et al. (2022) where single substrate and DO perturbations were imposed on the same strain, respectively. Meanwhile, the extracellular levels of central carbon metabolites under HOLG conditions showed marginal changes compared to control conditions (Figure 5A, Supporting Information S1: Figure 3). However, FBP and erythritol showed the largest decrease and increase in their extracellular concentrations, respectively.

At the 270-second point in the combined fluctuation cycle, extracellular conditions were closest to the control, marking the beginning of the HOLG scenario (Figure 1B, Supporting Information S1: Figure 3). Aside from the increase in intracellular FBP levels compared to the control, most metabolite levels in the upstream EMP pathway decreased (Figure 4B, Supporting Information S1: Figure 2). For example, intracellular levels of glucose, G6P, and F6P dropped by approximately 74.4%, 37.9%, and 19.1%, respectively. This indicates that glucose entering the cells during the high-glucose pulse was likely metabolized faster through the upstream EMP pathway. A similar phenomenon was observed in previous studies with *P. chrysogenum* during single substrate fluctuations (G. Wang et al. 2018) and combined glucose-oxygen fluctuations (Janoska et al. 2023). Induced by substrate concentration fluctuations. 6PG and S7P also decreased by about 47.5% and 23.4%, respectively, suggesting that carbon flux did not prefer to flow into the PP pathway. Intracellular trehalose levels were three times higher than the control, and the intracellular levels of other three sugar alcohols such as mannitol, arabitol and erythritol increased by 30%–50%. Hence, the cells prefer to synthesize large amounts of trehalose and sugar alcohols to cope with the GFGO conditions. The intracellular levels of citrate, α-ketoglutarate, succinate, fumarate, and malate in the TCA cycle decreased by 42.3%, 14.7%, 23.1%, 50.5%, and 38.8%, respectively. Due to a longer metabolic route away from the gate of the glucose influx, the TCA cycle did not respond as sensitively as the EMP pathway and PP pathway, or its response might be delayed. During the recovery phase, not all the metabolites can return to control levels. Notably, intracellular levels of glucose, FBP, arabitol, and fumarate were 64.1%, 38.4%, 43.2%, and 34.1% lower than the control, respectively, while M1P, mannitol, erythritol, and succinate levels increased by 34.4%, 14.2%, 23.5%, and 36.5%.

Intracellular glucose levels fluctuated within a single cycle, showing a rapid increase followed by a slower decrease, with a peak value during the HOLG phase (Figure 4C). G6P, F6P, and M6P followed a similar pattern, with peaks at around 180 s, approximately 1.75, 1.67, and 1.69 times higher than the control, respectively. These peaks lagged behind the extracellular substrate fluctuation peak, mainly because of the limited ATP generation caused by the low oxygen level (Figure 1B). FBP levels fluctuated less significantly than other EMP pathway metabolites, likely due to the energy-requiring phosphofructokinase reaction. Trehalose and the other three sugar alcohols showed consistently higher levels than the control, with two small peaks around 145 and 320 s, likely indicating a delayed metabolic response. In the TCA cycle, the intracellular level of α-ketoglutarate did not show a clear trend compared to succinate, fumarate, and malate, possibly due to the limitation of isocitrate dehydrogenase or a shift towards the glyoxylate shunt to reduce the generation of reducing equivalent (Yang et al. 2022).

At the 270th second of the combined fluctuation, all detected central carbon metabolites exhibited increased extracellular concentrations, except for FBP and mannitol (Figure 5B, Supporting Information S1: Figure 3). Specifically, the extracellular concentrations of G6P, M6P, M1P, S7P, and fumarate were almost doubled, while the extracellular concentrations of 6PG, succinate, and malate were over 10 times higher relative to the control. Most interestingly, the intracellular and extracellular concentrations of all metabolites in the EMP pathway, PP pathway, and TCA cycle, as well as M6P, M1P, and mannitol involved in storage metabolism, showed changes in opposite directions (Figures 4B and 5B). In addition to this, the intracellular and extracellular concentrations of trehalose and two other polyols simultaneously increased. Overall, these results are similar to those obtained under HGLO conditions, but the increase in metabolite concentrations relative to the control was smaller than in the former case. This suggests that the metabolite secretion may be related to the 45-second HGLO condition during the cycle. Carbon loss due to extracellular metabolite secretion was also observed during single oxygen fluctuations (Janoska et al. 2022; Yang et al. 2022). Compared to the results under HGLO conditions, the extracellular concentrations of all metabolites in the TCA cycle were within a relatively normal range, indicating that the temporal mismatch between substrate and oxygen availability under GFGO conditions did not lead to a severe blockade of the TCA cycle. Interestingly, the overaccumulation of α-ketoglutarate extracellularly was also observed, suggesting the importance of primary ammonium assimilation processes for microbial growth (Bernard and Habash 2009).

Substrate concentrations initially exceeded the excess threshold and then dropped below the starvation threshold during the

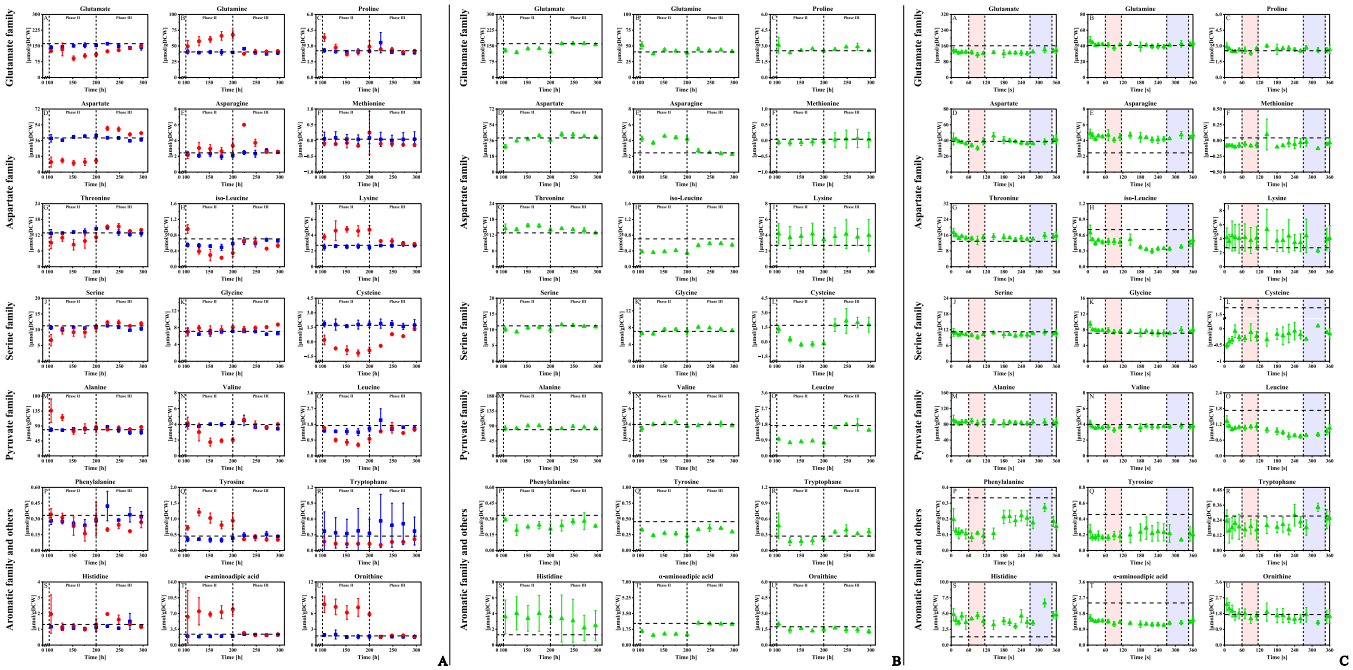

FIGURE 6 | Intracellular amounts of amino acids. (A) HGLO and HOLG; (B) GFGO long term; (C) GFGO single cycle. ▬ ▬ ▬ represents the mean value of the control. ● represents the mean value of HGLO. ■ represents the mean value of HOLG. ▲ represents the mean value of GFGO. Phase I, II, and III correspond to steady state, experimental, and recovery phases, respectively. Red rectangular area corresponds to HGLO. Blue rectangular area corresponds to HOLG. All error bars represent the standard deviation of data obtained from three independent biological replicates.

cycle (Figure 5C). Peaks appeared about 70 s into the cycle, 20 s later than in single substrate fluctuation studies (de Jonge et al. 2011), likely due to the effects of oxygen limitation on substrate transport. The overall pattern of extracellular metabolite fluctuations reflected the long-term trends. Except for FBP, whose extracellular levels were lower than the control, and mannitol, which remained unchanged, all other central carbon metabolites showed increased extracellular concentrations. Peaks in metabolite concentrations aligned with the extreme HGLO and HOLG conditions, suggesting that the extreme conditions might promote the excretion of central carbon metabolites.

3.3.3 | Amino Acid Metabolism

Under HGLO conditions, intracellular glutamate levels decreased by about 25%, while glutamine levels increased by approximately 48.5% compared to the control (Figure 6A, Supporting Information S1: Figure 4). The biosynthesis of these amino acids is closely linked to ammonium assimilation (Bernard and Habash 2009; Holmes et al. 1991), and they can be interconverted. Among the aspartate family amino acids, only asparagine increased by approximately 16.4%, while the levels of other amino acids decreased. This may be due to the reduced availability of glutamate, the precursor of aspartate. Intracellular serine levels decreased by about 20%, while its precursor, cysteine, was nearly depleted. This could be related to the reduction status of intracellular environment because the 3-phosphoglycerate (3PG) to serine pathway releases reducing power (Broeks et al. 2023). In the pyruvate family, valine and leucine levels decreased by approximately 35% and 43.9%, respectively, possibly due to the reduced availability of glutamate. The intracellular level of α-aminoadipic acid increased threefold compared to the control (Figure 6A, Supporting Information S1: Figure 4), which was consistent with the increased secretion of its cyclized product OPC (Figure 2A).

Under HOLG conditions, there are no significant changes in intracellular amino acid levels (Figure 6A), consistent with the VIP score results (Figure 3B). Only leucine, isoleucine and phenylalanine, showed significant decreases of approximately 17.9%, 25.3%, and 20.0%, respectively, compared to the control, while tryptophan levels increased by about 26.4%. These changes in aromatic amino acid levels suggest that the shikimate pathway was more inclined toward the biosynthesis of tryptophan.

Under GFGO conditions, intracellular glutamate levels decreased by about 20% compared to the control (Figure 6B, Supporting Information S1: Figure 4). Other amino acids in the glutamate family showed increases of less than 5%. In the aspartate family, intracellular asparagine and threonine levels increased by 72.9% and 15.1%, respectively, while intracellular aspartate and isoleucine levels decreased by 46.8% and 7.5%, and methionine levels approached zero. The increase in asparagine was previously observed in the combined fluctuation study by Janoska et al. (2023), but not in single substrate (G. Wang et al. 2018) or oxygen fluctuation experiments (Yang et al. 2022), suggesting that it is specific to combined fluctuations. Isoleucine levels followed the opposite trend to its precursor threonine and were similar to the trends in leucine, possibly due to competition for pyruvate as the precursor (Strassman et al. 1956) or shared enzymes like dihydroxy acid dehydratase (DHAD) and branched chain amino acid transaminase (BCAT) (Joel T. Steyer et al. 2021; Liang et al. 2021). In the serine family, cysteine levels decreased by 89.8%, which has been linked to carbon or nitrogen deprivation (Skye and Segel 1970). Given that

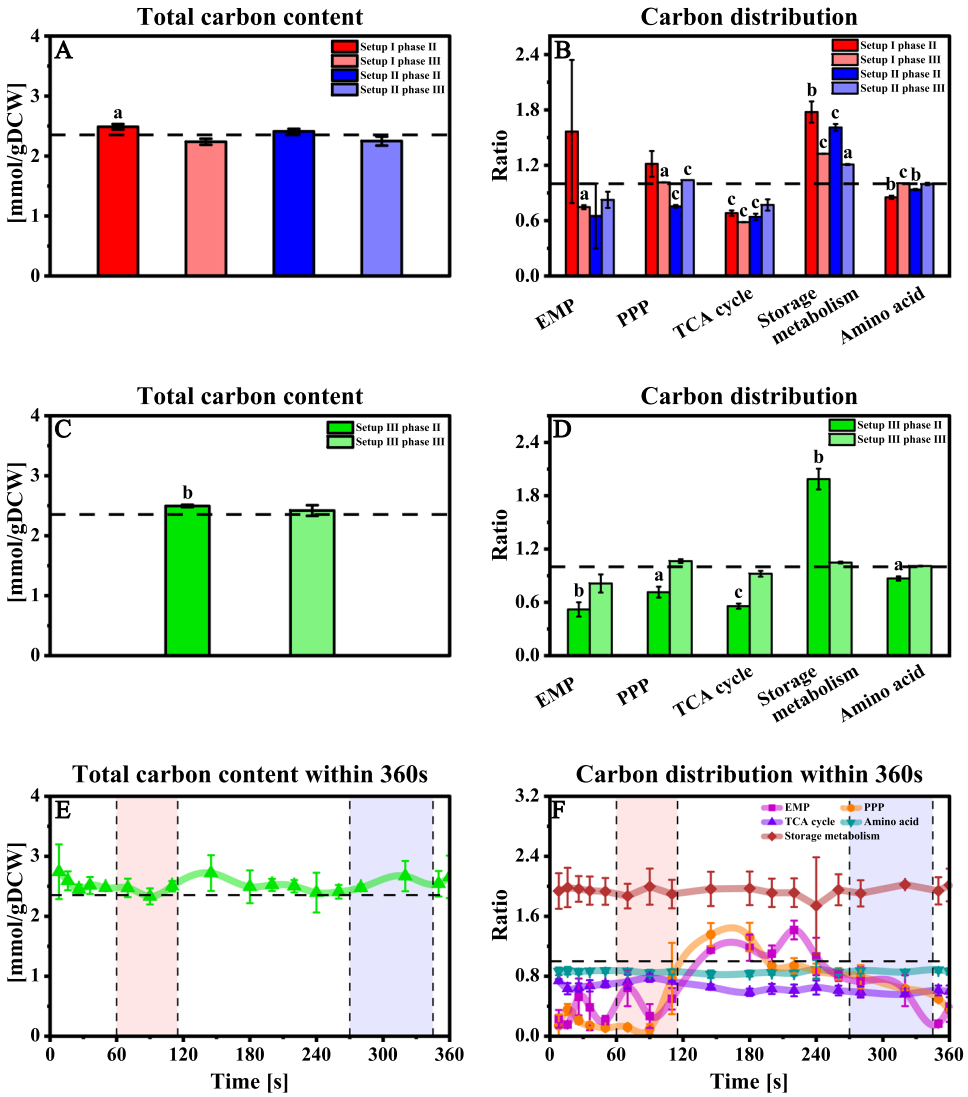

FIGURE 7 | Intracellular carbon distribution. A, B: HGLO and HOLG; C, D: GFGO long term; E, F: GFGO single cycle. ▬ ▬ ▬ represents normalized control. In *t*-test, $p < 0.05$, 0.01 and 0.005 are marked as a, b and c, respectively. Red rectangular area corresponds to HGLO. Blue rectangular area corresponds to HOLG. All error bars represent the standard deviation of data obtained from three independent biological replicates.

cells experienced glucose starvation for about 90 s during the 360-second combined fluctuation cycle, increased membrane permeability may lead to cysteine leakage. The intracellular levels of phenylalanine, tyrosine and tryptophan decreased by 30.6%, 41.3%, and 10.3%, respectively, likely due to a reduced carbon flux into the shikimate pathway (Shende et al. 2024). The concentrations of α-aminoadipate acid and lysine decreased and increased by approximately 48.2% and 42.4%, respectively. This is likely related to the feedback regulation mechanism of lysine metabolism in *P. chrysogenum*. It has been previously reported that penicillin production is highly sensitive to lysine availability. Excessive lysine levels can inhibit citrate synthase activity through feedback regulation, resulting in an insufficient supply of the precursor α-aminoadipate acid, which subsequently affects penicillin production (Goulden and Chattaway 1968).

The trends in intracellular amino acid levels during short cycles were consistent with long-term observations, although the magnitudes differ (Figure 6C). Most amino acids showed two peaks during the cycle, occurring at around 8 and 145 s, with the first peak generally being higher. Previous studies have shown that intracellular amino acid levels can respond to fluctuations in substrate or oxygen, and the peaks in amino acid levels corresponded to peaks in intracellular substrate or DO concentrations (G. Wang et al. 2018; Yang et al. 2022). In this study, the two peaks in amino acid levels were separated by about 137 s, suggesting that the first peak was linked to extracellular glucose levels, while the second corresponded to extracellular DO levels. This pattern resembles the behavior observed for succinate, fumarate, and malate in the TCA cycle, though the fluctuations in amino acid levels were smaller in comparison.

3.3.4 | Intracellular Carbon Distribution

Under HGLO conditions, the total intracellular carbon content increased by approximately 5.7% compared to the control (Figure 7A). The carbon content proportions of the EMP pathway, PP pathway, and storage metabolism increased by about 56.6%, 21.5%, and 77.7%, respectively, while the

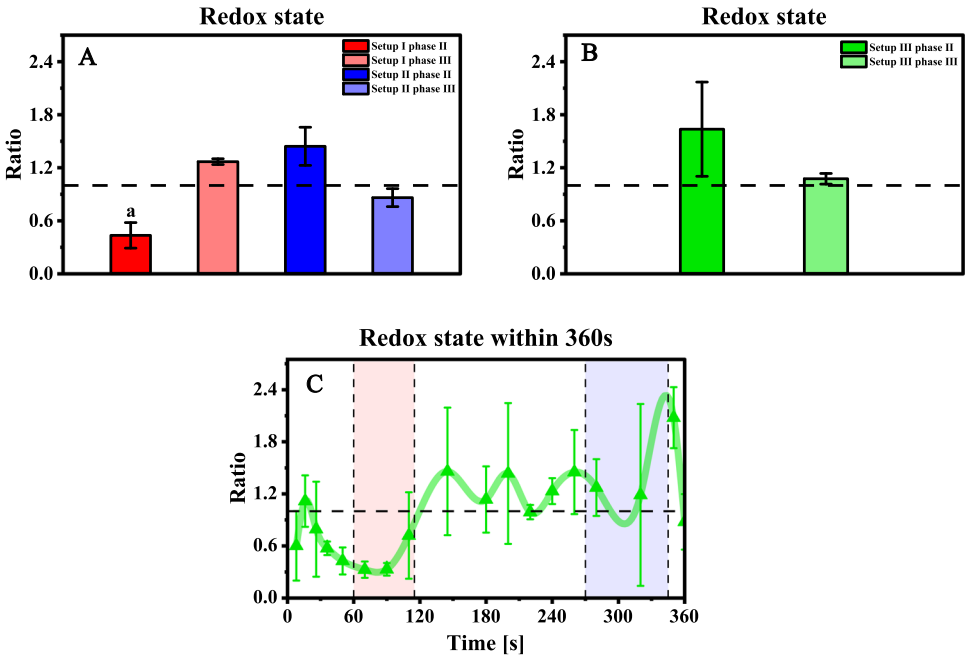

FIGURE 8 | Intracellular redox state (NAD^+/NADH). (A) HGLO and HOLG; (B) GFGO long term; (C) GFGO single cycle. ▬ ▬ ▬ represents normalized control. In *t*-test, $p < 0.05$ is marked as a. ▲ represents the mean value of GFGO. All error bars represent the standard deviation of data obtained from three independent biological replicates.

proportions of the TCA cycle and amino acid metabolism decreased by 31.9% and 11.7%. These results suggest that more carbon was directed into the PP pathway and storage carbon pools (Figure 7B). During the recovery phase, carbon flow remained primarily directed toward the PP pathway and storage metabolism, suggesting that the cells retained a "memory" of the previous stress (Lambert and Kussell 2014).

Under HOLG conditions, the total intracellular carbon content increased by approximately 2.5% compared to the control (Figure 7A). Only the proportion of carbon in storage metabolism showed a significant increase of about 60.9% (Figure 7B). In response to intermittent substrate limitation and starvation, the cells synthesized more storage metabolites to maintain metabolic stability during starvation periods. Although penicillin productivity did not show a significant decline, the reduced biomass concentration (Table 1) as well as decreased carbon content in the EMP pathway and TCA cycle indicated an energy metabolic burden. Moreover, this alteration was not fully reversed during the recovery phase.

At the 270-second point in the combined fluctuation cycle, total intracellular carbon content increased by about 6.0% compared to the control (Figure 7C). Most of the carbon was converted to storage metabolites, with the proportion of storage carbon pool about twice that of the control. Carbon distribution to the EMP pathway, PP pathway, TCA cycle, and amino acid metabolism decreased by approximately 48%, 28%, 44%, and 13%, respectively (Figure 7D). This indicates that at this point, intracellular carbon rapidly inflowed through the EMP pathway and PP pathway but did not enter the TCA cycle or amino acid metabolism. Instead, it accumulated in storage metabolites, preparing the cells for the upcoming 90-second substrate starvation period. Similar phenomena were observed by Janoska et al. (2022). However, the significant carbon accumulation in storage metabolites could create an energy gap, as the futile cycling of storage metabolism consumes additional energy (de Jonge et al. 2014), which may partially explain the reduced penicillin production under these conditions. During the recovery phase, total intracellular carbon content increased by about 2.8% compared to the control. The proportions of carbon in the EMP pathway and TCA cycle decreased by 18.7% and 7.8%, while the proportions in the PP pathway and amino acid pathways increased by 6.4% and 4.8%, respectively. Carbon distribution in the recovery phase resembled the distribution under HOLG conditions, with no observable metabolic irreversibility or signs of cell decline (Figure 2A). This may be due to the absence of excess substrate periods under HOLG conditions, which prevented the cells from synthesizing sufficient storage carbon to sustain them during the 30-second starvation period later in the cycle.

Under GFGO conditions, the intracellular total carbon content remained higher than the control throughout the short cycle, with the cycle-averaged content exceeding the control by approximately 7.3% (Figure 7E,F). There was a noticeable trend in carbon distribution within the EMP pathway and PP pathway, where the peak proportions of carbon occurred during periods when neither substrate nor oxygen was limiting. These peaks lagged behind the substrate concentration peaks by more than 1 min, likely due to the accumulation of extracellular substrate that could not immediately enter the cell for metabolism under oxygen-limited conditions. In contrast, the carbon distribution in the TCA cycle, storage metabolism, and amino acid metabolism remained relatively stable without significant variation. Except for the average carbon proportion in storage metabolism, which was nearly double that of the control, the average carbon content proportions in other carbon pools were lower than those in the control. The fluctuations in the TCA cycle carbon content were much smaller than those in the EMP

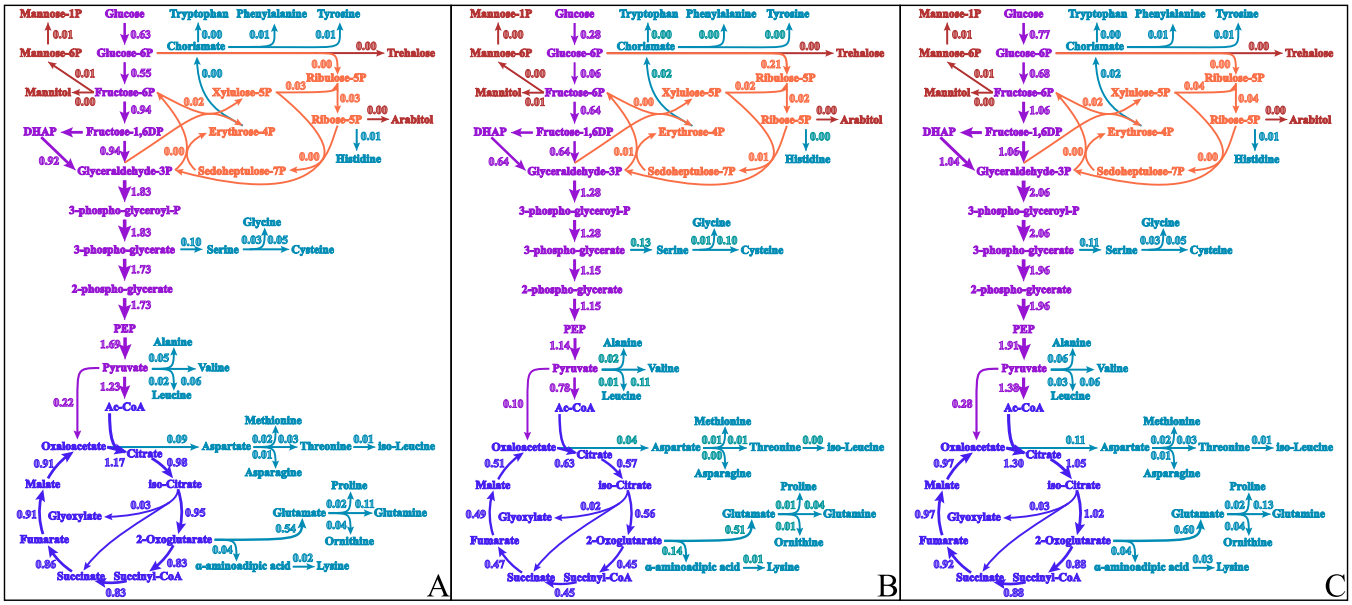

FIGURE 9 | Intracellular metabolic flux. (A) represents control. (B) represents HGLO. (C) represents HOLG. represents EMP pathway. represents PP pathway. represents TCA cycle. represents storage metabolism. represents amino acid pathway.

pathway. This appears reasonable that the longer metabolic pathway dampened the fluctuations in metabolite concentrations. Meanwhile, a subtle peak in the carbon content proportion of the TCA cycle was observed, occurring almost simultaneously with the extracellular substrate concentration peak. This suggests that the cell response to the external environmental fluctuations in the previous cycle required about 240 s to manifest in the TCA cycle. Similar delays were observed in studies on single oxygen concentration fluctuations, but the delay reported by Yang et al. (2022) was shorter, possibly due to their shorter fluctuation periods. The proportion of carbon in storage metabolism remained consistently high, likely due to the need for large amounts of stored metabolites to maintain cellular metabolic stability, which was consistent with the findings of G. Wang et al. (2018). During the 360-second combined fluctuation cycle, there was a substrate starvation period lasting nearly 90 s, during which the cells likely broke down previously synthesized storage carbohydrates to provide energy (de Jonge et al. 2014). A low point in the proportion of carbon in storage metabolism was observed when the extracellular substrate concentration was depleted, possibly marking the onset of catabolism.

3.3.5 | Cytoplasmic Redox State

Under HGLO conditions, the cytoplasm was significantly more reduced (indicated by NADH/NAD^+ ratio) than under control conditions, while the opposite was true under HOLG conditions (Figure 8A). During the recovery phases, the intracellular redox states were reversed from their respective experimental periods. Reports have shown that cytoplasmic reduction is negatively correlated with penicillin production (Goulden and Chattaway 1968; Harris et al. 2006), as the folding of key enzymes involved in penicillin biosynthesis—tripeptide synthetase, isopenicillin N synthase, and isopenicillin N acyltransferase—and the expression of related genes are impaired under these conditions. This observation is also reflected in this study (Figure 8A).

At the 270-second point in the combined fluctuation cycle, cytoplasmic oxidation state was significantly higher than the control, though the difference was not statistically significant (Figure 8B). During the recovery phase, cytoplasmic oxidation state was also slightly higher than the control, without significant differences. The redox state fluctuated throughout the 360-second cycle, closely following changes in the extracellular environment (Figure 8C). Cytoplasmic reduction state increased during HGLO periods, while oxidation state increased during HOLG periods, corresponding to high substrate and oxygen availability conditions, respectively. Taken together, the combined effects of substrate and oxygen fluctuations amplify their impact on the cytoplasmic redox state.

3.3.6 | Intracellular Metabolic Flux

Under HGLO conditions, the metabolic flux through the EMP pathway and TCA cycle decreased by approximately 30% and 50%, respectively, compared to the control (Figure 9A,B). This overall reduction in flux through the main energy metabolic pathways is consistent with the fact that cells experience energy metabolic disorders. The flux through the glyoxylate shunt did not increase as much as reported by Yang et al. (2022), but its proportion of the total TCA cycle flux did increase. This suggests that under low-oxygen conditions, cells altered their metabolic pathways to reduce the production of reducing power, which is consistent with the higher intracellular reduced state described in Section 3.3.5. The flux through the PP pathway increased significantly at the entry point but decreased within the pathway compared to the control. The flux associated with storage metabolism showed no significant difference from the control. In amino acid metabolism, only the flux towards serine, cysteine, valine, and α-aminoadipate acid

increased by approximately 30%, one-fold, one-fold, and two-fold, respectively, while the flux through other amino acid synthesis pathways decreased compared to the control. The increased flux into the PP pathway and toward cysteine, valine, and α-aminoadipate acid suggests that the cells seem to prioritize NADPH production and precursor amino acids required for penicillin G synthesis. This seems reasonable that due to the oxygen limitation, cells were unable to efficiently convert PAA to *o*-OH-PAA for detoxification, and thus they favored penicillin G biosynthesis. However, under HGLO conditions, it is obvious that the impaired penicillin production capacity is not capable of being used for detoxification purpose (Figure 2A). A previous study has reported that PAA can be efficiently taken up by the cell via passive diffusion and meanwhile actively excreted at the expense of extra ATP (Douma et al. 2012). Taken together, the results imply that this futile cycling of PAA may be further enhanced, which likely aggravates the energy deficit of *P. chrysogenum* cells under HGLO conditions.

Under HOLG conditions, the metabolic flux through the EMP pathway and TCA cycle increased by approximately 10%–20% (Figure 9A,C), corresponding to the increase in glucose-specific consumption rate (Table 1). The flux from ribose-5-phosphate to xylulose-5-phosphate and ribulose-5-phosphate in the PP pathway increased by about 25%, while other reactions showed no significant changes. The flux associated with storage metabolism showed no significant difference from the control. In amino acid metabolism, the flux towards branched-chain amino acids, serine, alanine, leucine, aspartate, glutamate, glutamine, and lysine slightly increased, while other synthesis pathways remained unchanged. The changes in amino acid metabolic flux may be related to the increased demand for transport proteins required to cope with fluctuating substrate conditions. G. Wang et al. (2018) reported that very low extracellular glucose concentrations may induce the expression of genes encoding high-affinity glucose transporters. Such conditions were present in this study under HOLG conditions, where approximately 70 s of each fluctuation cycle experienced near-zero extracellular glucose concentrations (Figure 2A).

Under GFGO conditions, the first reaction in the EMP pathway mirrored changes in extracellular glucose levels (Figure 10), with flux peaking during substrate excess, followed by a plateau and a gradual decline as substrate levels decreased. Most EMP pathway reactions showed similar trends, with flux peaks following extracellular substrate and DO peaks, suggesting that high concentrations of both promote glycolytic flux. The flux of FBP differed from other EMP pathway reactions, likely due to diversion into the PP pathway. TCA cycle fluxes for citrate, isocitrate, and α-ketoglutarate followed similar trends to the EMP pathway. The glyoxylate shunt showed more distinct peaks corresponding to substrate and oxygen concentration peaks, likely because this pathway is not influenced by energy or reducing power (Lara et al. 2006; Yang et al. 2022). In contrast, fluxes for succinate, fumarate, and malate declined steadily, reflecting their dependence on oxygen availability and cytoplasmic redox balance, with flux peaks occurring after oxygen concentration peaks at the end of each cycle. PP pathway reactions shared metabolites with the EMP pathway, such as xylulose-5-phosphate and erythrose-4-phosphate, and exhibited similar double-peak trends, though delayed by about 60 s, likely due to the reduced cytoplasmic redox state at the start of the cycle. Trehalose synthesis showed significant flux during the substrate starvation period at the start of each cycle, indicating the cell response to nutrient deprivation (de Jonge et al. 2014). The fluxes of most amino acids followed the trends of their precursors, with flux peaks dependent on whether reducing power or energy was required.

3.4 | Implications for Large-Scale Fermentation

Due to mixing and mass transfer limitations in large-scale reactors, a variety of gradients, including substrate, DO, and pH are induced. Microorganisms need to carefully evolve metabolic strategies to cope with the heterogeneous environment as they move through different zones within the bioreactor. During industrial penicillin fermentation, fluctuations in substrate, and oxygen availability have been proven to have a significant impact on the physiological state and penicillin production of *P. chrysogenum* (G. Wang et al. 2018; X. Wang et al. 2024; Zhao et al. 2024). The scale-down philosophy examines broth heterogeneity affects process performance by considering its impact early in development (Neubauer and Junne 2010). A key challenge is creating a lab-scale environment that accurately reflects industrial broth heterogeneity, essential for understanding cellular metabolic responses. However, data on glucose and DO levels for the 54 m^3 penicillin bioreactor is lacking. Since the pioneering work of Lapin (Lapin et al. 2004), Euler-Lagrange CFD has been used to simulate the hydrodynamics of large-scale bioreactors. While experimental validation of CFD predictions at an industrial scale remains difficult, CFD simulations provide valuable insights into the microbial environment. This study assumes that CFD models accurately predict gradients in the full-scale bioreactor (Haringa et al. 2016; Wei et al. 2023), along with the limited DO data available from a similar penicillin process (X. Wang et al. 2024). Accordingly, *P. chrysogenum* cells are long-term exposed to HGLO (near the feed inlet) or HOLG (below the top impeller), or they alternate between HGLO and HOLG conditions over timescales of seconds to minutes in the bioreactor.

Our scale-down studies have shown that if *P. chrysogenum* cells suffer from combined gradients of substrate and DO in different zones of the bioreactor at large-scale, drastic changes in metabolite level, flux distribution and thus penicillin production capacity were observed. Specifically, the results indicate that prolonged exposure to HGLO zone (near the feed inlet point) could lead to a complete loss of penicillin production capacity, which can be partially recovered as the cells move into DO-unlimited zones. Cells randomly walking through HOLG zone (near the aeration point) seldomly experience any loss of production capacity but may undergo premature degeneration due to increased energy burden. When cells are forced by the fluid flow to experience GFGO conditions in the large-scale bioreactor, the penicillin productivity is almost halved. Based on the current experimental findings, it can be concluded that *P. chrysogenum* cells demonstrate a degree of adaptability to substrate gradients, as these do not necessarily result in irreversible effects on production, although large gradients may reduce productivity. In contrast, oxygen gradients have a more pronounced negative impact, not only reducing overall production but also potentially causing irreversible damage to the cells. These results highlight that while the strain can tolerate some

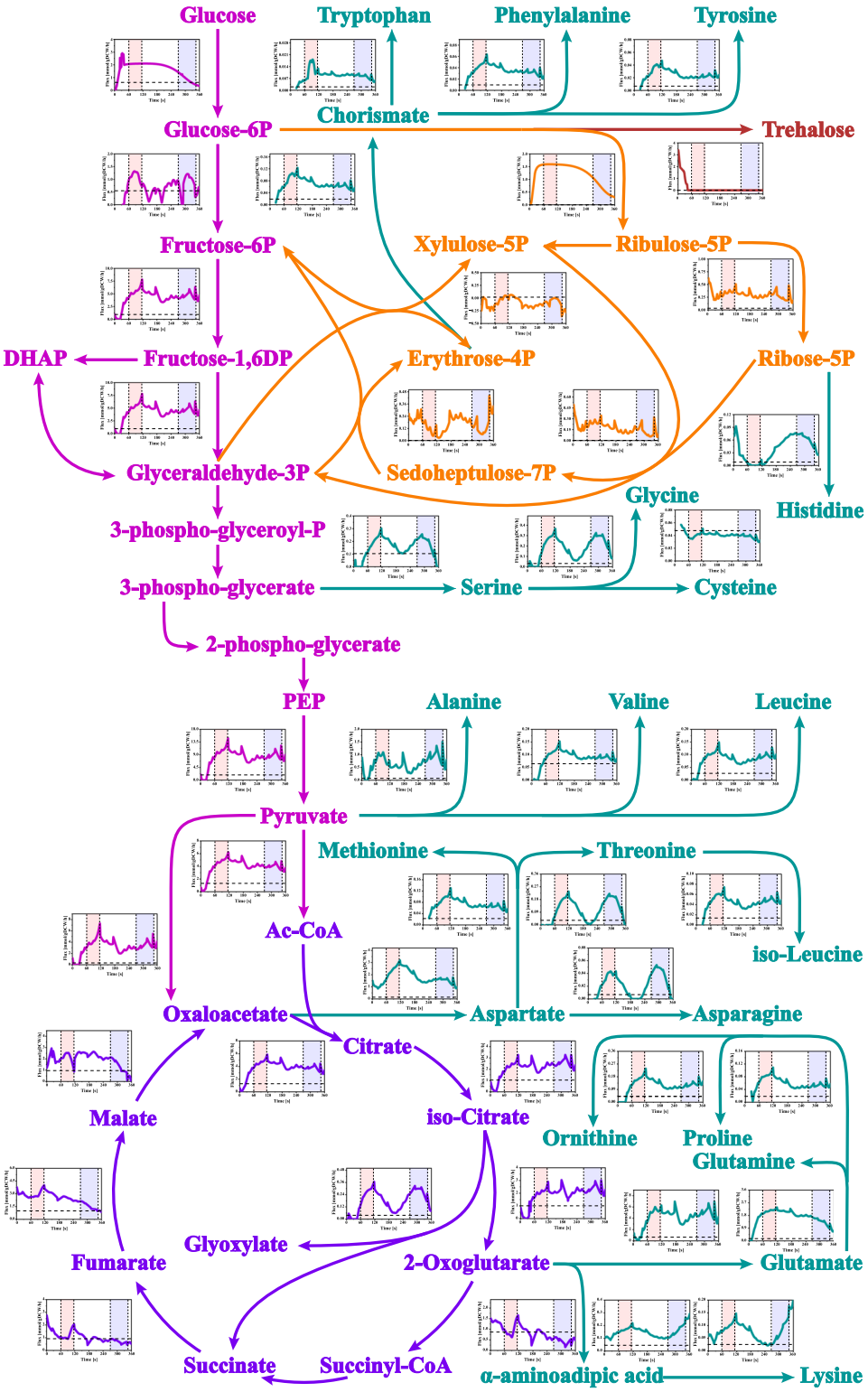

FIGURE 10 | Intracellular metabolic flux within the oscillation cycle under GFGO conditions. ——— represents EMP pathway. ——— represents PP pathway. ——— represents TCA cycle. ——— represents storage metabolism. ——— represents amino acid pathway.

perturbations in substrate concentration, maintaining oxygen levels within an optimal range is crucial for maximizing productivity and preventing cell damage.

In industrial practice, it is common to rely on a single DO measurement recorded by a DO probe at the bottom of the bioreactor to evaluate the oxygen supply. However, due to reduced availability of substrate and the higher hydrostatic pressure at the bottom, the recorded DO value in an industrial-scale bioreactor can be two to four times higher than at the top. Clearly, measuring DO at only one location in the bioreactor is insufficient for large-scale operations. Therefore, in large-scale penicillin

fermentation, it is advisable to monitor DO levels at multiple points within the bioreactor and implement adaptive control strategies (e.g., adjusting agitation/aeration rates) to prevent oxygen limitation throughout the entire system. In cases where oxygen limitation occurs near the HGLO zone, expressing recombinant bacterial hemoglobin could potentially help mitigate undesirable side effects (Hofmann et al. 2009). Additionally, to reduce substrate gradients, the substrate feed could be repositioned from the top to the impeller discharge stream or supplemented with additional feed points at the middle and bottom of the bioreactor (Haringa et al. 2018). Furthermore, replacing the glucose uptake system with one that has a lower affinity for glucose may further help to stabilize conditions. Together, these strategies can reduce extreme oscillations in substrate and DO levels, minimizing heterogeneities in biomass growth and improving overall production performance.

3.5 | Limitations and Opportunities for Further Study

Although this study provides valuable insights into the impact of said heterogeneity on cellular responses in a scale-down model, it has limitations in accurately replicating the "history" of perturbations and high cell-density conditions typical of industrial-scale bioreactors. Specifically, the use of a chemostat at low cell density and short-duration perturbations may not fully capture the "history" of cyclic exposure to nutrient and oxygen heterogeneities, nor the long-term effects this "history" has on cellular responses in large-scale processes.

To address the concerns regarding the impact of "history" on cellular responses, we propose a more refined experimental approach. Specifically, we suggest using a high cell-density fed-batch fermentation system with exponential feeding to maintain a fixed specific biomass growth rate. This would allow for the controlled, continuous exposure of cells to dynamic nutrient and oxygen fluctuations, closely mimicking the "history" of perturbations that cells experience in industrial-scale reactors, where cells are cyclically exposed to heterogeneities without leaving the vessel. To capture the effect of this "history" on cellular behavior, we propose integrating genetically encoded fluorescent sensors. These sensors would enable real-time monitoring of metabolic and stress-related responses, such as glucose consumption or reactive oxygen species (ROS) production, as the cells are exposed to fluctuating conditions over time. Furthermore, single-cell Raman spectroscopy could be used to examine how individual cells retain the "memory" of past perturbations, revealing how prior exposure to heterogeneities influences their current metabolic state and overall performance. Based on this, we can more effectively study the role of "perturbation history" in cellular responses, providing a clearer understanding of how cells adapt to the dynamic conditions of industrial-scale processes.

4 | Conclusion

In industrial-scale practice, it is of utmost importance to address the critical scientific question of how and to what extent local and global gradients of substrate and DO affect cell metabolism and bioprocess performance. Motivated by this, in this study, the said heterogeneous environments experienced by *P. chrysogenum* cells in an industrial-scale penicillin bioreactor were successfully mimicked in our sophisticated scale-down systems. Specially, local HGLO and HOLG conditions as well as GFGO conditions were used to simulate the substrate and DO concentration gradients in the feed inlet zone, aeration zone, and global environment at large-scale, respectively. The results indicated that the HGLO condition exerted the most significant impact on cellular metabolism, leading to substantial carbon loss. Prolonged exposure to the feed inlet region could result in the irreversible loss of penicillin production capacity. While the HOLG condition exerted little effect on penicillin production, it may increase the energy burden of cells, potentially causing premature degeneration for those circulating in the lower regions of the reactor. As the cells periodically experience the combined gradients, the results indicated that the presence of substrate gradients did not cause irreversible effects on production, but large substrate gradients indeed contributed to reduced productivity. While, the presence of oxygen gradients not only led to productivity loss but also induced irreversible damage to the cells.

Author Contributions

Conceptualization: Yining Chen, Guan Wang. Formal analysis: Yining Chen, Guan Wang. Investigation: Yining Chen. Writing-original draft preparation: Yining Chen. Editing: Yining Chen, Cees Haringa, Guan Wang. Project administration: Guan Wang, Zejiang Wang, Yingping Zhuang. Funding acquisition: Guan Wang, Yingping Zhuang.

Acknowledgments

This research was funded by the National Key R&D Program of China (Grant no. 2021YFC2101000), National Natural Science Foundation of China (Grant no. 31900073, 21978085), Shanghai Rising-Star Program (Grant no. 21QA1402400), Natural Science Foundation of Shanghai (Grant no. 19ZR1413600), and the Fundamental Research Funds for the Central Universities (Grant No. JKF01241708).

Conflicts of Interest

The authors declare no conflicts of interest.

Data Availability Statement

The authors declare that the data supporting the findings of this study are available within the paper. If raw data files are needed in another format, they are available from the corresponding author upon reasonable request. The data that support the findings of this study are available from the corresponding author upon reasonable request.

References

Arcus, A. C., and N. L. Edson. 1956. "Polyol Dehydrogenases. 2. The Polyol Dehydrogenases Of *Acetobacter suboxydans* And *Candida utilis*." *Biochemical Journal* 64, no. 3: 385–394. https://doi.org/10.1042/bj0640385.

Bainbridge, Z. A., R. I. Scott, and D. Perry. 2007. "Oxygen Utilisation by Isopenicillin N Synthase From *Penicillium chrysogenum*." *Journal of Chemical Technology & Biotechnology* 55, no. 3: 233–238. https://doi.org/10.1002/jctb.280550306.

Bernard, S. M., and D. Z. Habash. 2009. "The Importance of Cytosolic Glutamine Synthetase in Nitrogen Assimilation and RecJongeycling." *New Phytologist* 182, no. 3: 608–620. https://doi.org/10.1111/j.1469-8137.2009.02823.x.

Bhargava, S., M. P. Nandakumar, A. Roy, K. S. Wenger, and M. R. Marten. 2003. "Pulsed Feeding During Fed-Batch Fungal Fermentation Leads to Reduced Viscosity Without Detrimentally Affecting Protein Expression." *Biotechnology and Bioengineering* 81, no. 3: 341–347. https://doi.org/10.1002/bit.10481.

Bhargava, S., K. S. Wenger, and M. R. Marten. 2003a. "Pulsed Addition of Limiting-Carbon During *Aspergillus oryzae* Fermentation Leads to Improved Productivity of a Recombinant Enzyme." *Biotechnology and Bioengineering* 82, no. 1: 111–117. https://doi.org/10.1002/bit.10548.

Bhargava, S., K. S. Wenger, and M. R. Marten. 2003b. "Pulsed Feeding During Fed-Batch *Aspergillus oryzae* Fermentation Leads to Improved Oxygen Mass Transfer." *Biotechnology Progress* 19, no. 3: 1091–1094. https://doi.org/10.1021/bp025694p.

Broeks, M. H., N. W. F. Meijer, D. Westland, et al. 2023. "The Malate-Aspartate Shuttle Is Important for De Novo Serine Biosynthesis." *Cell Reports* 42, no. 9: 113043. https://doi.org/10.1016/j.celrep.2023.113043.

Buchholz, J., M. Graf, A. Freund, et al. 2014. "CO_2/HCO_3^- Perturbations of Simulated Large Scale Gradients in a Scale-Down Device Cause Fast Transcriptional Responses in *Corynebacterium glutamicum*." *Applied Microbiology and Biotechnology* 98, no. 20: 8563–8572. https://doi.org/10.1007/s00253-014-6014-y.

Bylund, F., E. Collet, S. O. Enfors, and G. Larsson. 1998. "Substrate Gradient Formation in the Large-Scale Bioreactor Lowers Cell Yield and Increases By-Product Formation." *Bioprocess Engineering* 18, no. 3: 171–180. https://doi.org/10.1007/s004490050427.

Deshmukh, A. T., P. J. T. Verheijen, R. Maleki Seifar, J. J. Heijnen, and W. M. van Gulik. 2015. "In Vivo Kinetic Analysis of the Penicillin Biosynthesis Pathway Using PAA Stimulus Response Experiments." *Metabolic Engineering* 32, no. 1: 155–173. https://doi.org/10.1016/j.ymben.2015.09.018.

Douma, R. D., A. T. Deshmukh, L. P. de Jonge, et al. 2012. "Novel Insights in Transport Mechanisms and Kinetics of Phenylacetic Acid and Penicillin-G in *Penicillium chrysogenum*." *Biotechnology Progress* 28, no. 2: 337–348. https://doi.org/10.1002/btpr.1503.

Douma, R. D., P. J. T. Verheijen, W. T. A. M. de Laat, J. J. Heijnen, and W. M. van Gulik. 2010. "Dynamic Gene Expression Regulation Model for Growth and Penicillin Production in *Penicillium chrysogenum*." *Biotechnology and Bioengineering* 106, no. 4: 608–618. https://doi.org/10.1002/bit.22689.

Goulden, S. A., and F. W. Chattaway. 1968. "Lysine Control of α-Aminoadipate and Penicillin Synthesis in *Penicillium chrysogenum*." *Biochemical Journal* 110, no. 4: 55P–56P. https://doi.org/10.1042/bj1100055P.

van Gulik, W. M., W. T. A. M. de Laat, J. L. Vinke, and J. J. Heijnen. 2000. "Application of Metabolic Flux Analysis for the Identification of Metabolic Bottlenecks in the Biosynthesis of Penicillin-G." *Biotechnology and Bioengineering* 68, no. 6: 602–618.

Haringa, C., W. Tang, A. T. Deshmukh, et al. 2016. "Euler-Lagrange Computational Fluid Dynamics for (Bio)Reactor Scale Down: An Analysis of Organism Lifelines." *Engineering in Life Sciences* 16, no. 7: 652–663. https://doi.org/10.1002/elsc.201600061.

Haringa, C., W. Tang, G. Wang, et al. 2018. "Computational Fluid Dynamics Simulation of an Industrial *P. chrysogenum* Fermentation With a Coupled 9-pool Metabolic Model: Towards Rational Scale-Down and Design Optimization." *Chemical Engineering Science* 175: 12–24. https://doi.org/10.1016/j.ces.2017.09.020.

Harris, D., J. Diderich, and Z. van der Krogt, et al. 2006. "Enzymic Analysis of NADPH Metabolism in β-Lactam-Producing *Penicillium chrysogenum*: Presence of a Mitochondrial NADPH Dehydrogenase." *Metabolic Engineering* 8, no. 2: 91–101. https://doi.org/10.1016/j.ymben.2005.09.004.

Henriksen, C. M., J. Nielsen, and J. Villadsen. 1998. "Cyclization Of.Alpha.-Aminoadipic Acid Into The.Delta.-Lactam 6-Oxo-Piperidine-2-Carboxylic Acid by *Penicillium chrysogenum*." *Journal of Antibiotics* 51, no. 2: 99–106. https://doi.org/10.7164/antibiotics.51.99.

Hofmann, G., A. Diano, and J. Nielsen. 2009. "Recombinant Bacterial Hemoglobin Alters Metabolism of *Aspergillus niger*." *Metabolic Engineering* 11, no. 1: 8–12. https://doi.org/10.1016/j.ymben.2008.07.002.

Holmes, A. R., G. S. Mcnaughton, R. D. More, and M. G. Shepherd. 1991. "Ammonium Assimilation by *Candida albicans* and Other Yeasts: a ^{13}N Isotope Study." *Canadian Journal of Microbiology* 37, no. 3: 226–232. https://doi.org/10.1139/m91-034.

Jami, M.-S., C. Barreiro, C. García-Estrada, and J.-F. Martín. 2010. "Proteome Analysis of the Penicillin Producer *Penicillium chrysogenum*." *Molecular & Cellular Proteomics* 9, no. 6: 1182–1198. https://doi.org/10.1074/mcp.M900327-MCP200.

Janoska, A., J. Buijs, and W. M. van Gulik. 2023. "Predicting the Influence of Combined Oxygen and Glucose Gradients Based On Scale-Down and Modelling Approaches for the Scale-Up of Penicillin Fermentations." *Process Biochemistry* 124, no. 1: 100–112. https://doi.org/10.1016/j.procbio.2022.11.006.

Janoska, A., J. J. Verheijen, W. Tang, Q. Lee, B. Sikkema, and W. M. van Gulik. 2022. "Influence of Oxygen Concentration on the Metabolism of *Penicillium chrysogenum*." *Engineering in Life Sciences* 23, no. 1: e210013. https://doi.org/10.1002/elsc.202100139.

de Jonge, L., N. A. A. Buijs, J. J. Heijnen, W. M. van Gulik, A. Abate, and S. A. Wahl. 2014. "Flux Response of Glycolysis and Storage Metabolism During Rapid Feast/Famine Conditions in *Penicillium chrysogenum* Using Dynamic ^{13}C Labeling." *Biotechnology Journal* 9, no. 3: 372–385. https://doi.org/10.1002/biot.201200260.

de Jonge, L. P., N. A. A. Buijs, A. ten Pierick, et al. 2011. "Scale-Down of Penicillin Production in *Penicillium chrysogenum*." *Biotechnology Journal* 6, no. 8: 944–958. https://doi.org/10.1002/biot.201000409.

Kampers, L. F. C., E. Asin-Garcia, P. J. Schaap, A. Wagemakers, and V. A. P. Martins dos Santos. 2021. "From Innovation to Application: Bridging the Valley of Death in Industrial Biotechnology." *Trends in Biotechnology* 39, no. 12: 1240–1242. https://doi.org/10.1016/j.tibtech.2021.04.010.

Kuschel, M., and R. Takors. 2020. "Simulated Oxygen and Glucose Gradients as a Prerequisite for Predicting Industrial Scale Performance a Priori." *Biotechnology and Bioengineering* 117, no. 9: 2760–2770. https://doi.org/10.1002/bit.27457.

Lambert, G., and E. Kussell. 2014. "Memory and Fitness Optimization of Bacteria Under Fluctuating Environments." *PLoS Genetics* 10, no. 9: e1004556. https://doi.org/10.1371/journal.pgen.1004556.g001.

Lapin, A., D. Muller, and M. Reuss. 2004. "Dynamic Behavior of Microbial Populations in Stirred Bioreactors Simulated With Euler-Lagrange Methods: Traveling Along the Lifelines of Single Cells." *Industrial & Engineering Chemistry Research* 43, no. 16: 4647–4656. https://doi.org/10.1021/ie030786k.

Lara, A. R., L. Leal, N. Flores, G. Gosset, F. Bolívar, and O. T. Ramírez. 2006. "Transcriptional and Metabolic Response of Recombinant *Escherichia coli* to Spatial Dissolved Oxygen Tension Gradients Simulated in a Scale-Down System." *Biotechnology and Bioengineering* 93, no. 2: 372–385. https://doi.org/10.1002/bit.20704.

Larsson, G., M. Törnkvist, E. Wernersson, C. Trägärdh, H. Noorman, and S. O. Enfors. 1996. "Substrate Gradients in Bioreactors: Origin and Consequences." *Bioprocess Engineering* 14, no. 6: 281–289. https://doi.org/10.1007/BF00369471.

Li, C., W. Shu, S. Wang, et al. 2018. "Dynamic Metabolic Response of *Aspergillus niger* to Glucose Perturbation: Evidence of Regulatory Mechanism for Reduced Glucoamylase Production." *Journal of Biotechnology* 287, no. 1: 28–40. https://doi.org/10.1016/j.jbiotec.2018.08.005.

Liang, Y.-F., Z.-X. Long, Y.-J. Zhang, et al. 2021. "The Chemical Mechanisms of the Enzymes in the Branched-Chain Amino Acids Biosynthetic Pathway and Their Applications." *Biochimie* 184, no. 1: 72–87. https://doi.org/10.1016/j.biochi.2021.02.008.

Linton, J. D., and W. Xu. 2021. "Understanding and Managing the Biotechnology Valley of Death." *Trends in Biotechnology* 39, no. 2: 107–110. https://doi.org/10.1016/j.tibtech.2020.06.013.

Liu, X., X. Sun, W. He, X. Tian, Y. Zhuang, and J. Chu. 2019. "Dynamic Changes of Metabolomics and Expression of Candicidin Biosynthesis Gene Cluster Caused by the Presence of a Pleiotropic Regulator Adpa in Streptomyces Zyj-6." *Bioprocess and Biosystems Engineering* 42, no. 8: 1353–1365. https://doi.org/10.1007/s00449-019-02135-4.

Liu, Z., and R. A. Butow. 2006. "Mitochondrial Retrograde Signaling." *Annual Review of Genetics* 40, no. 1: 159–185. https://doi.org/10.1146/annurev.genet.40.110405.090613.

Mashego, M., M. Jansen, J. Vinke, W. van Gulik, and J. Heijnen. 2005. "Changes in the Metabolome of Associated With Evolution in Aerobic Glucose-Limited Chemostats." *FEMS Yeast Research* 5, no. 4–5: 419–430. https://doi.org/10.1016/j.femsyr.2004.11.008.

Mu, Q., S. Zhang, X. Mao, Y. Tao, and B. Yu. 2021. "Highly Efficient Production of L-Homoserine in *Escherichia coli* by Engineering A Redox Balance Route." *Metabolic Engineering* 67, no. 1: 321–329. https://doi.org/10.1016/j.ymben.2021.07.011.

Nadal-Rey, G., D. D. McClure, J. M. Kavanagh, et al. 2021. "Development of Dynamic Compartment Models for Industrial Aerobic Fed-Batch Fermentation Processes." *Chemical Engineering Journal* 420, no. 3: 130402. https://doi.org/10.1016/j.cej.2021.130402.

Nadal-Rey, G., D. D. McClure, J. M. Kavanagh, S. Cornelissen, D. F. Fletcher, and K. V. Gernaey. 2021. "Understanding Gradients in Industrial Bioreactors." *Biotechnology Advances* 46: 107660. https://doi.org/10.1016/j.biotechadv.2020.107660.

Nasution, U., W. M. van Gulik, R. J. Kleijn, W. A. van Winden, A. Proell, and J. J. Heijnen. 2006. "Measurement of Intracellular Metabolites of Primary Metabolism and Adenine Nucleotides in Chemostat Cultivated *Penicillium chrysogenum*." *Biotechnology and Bioengineering* 94, no. 1: 159–166. https://doi.org/10.1002/bit.20842.

Neubauer, P., and S. Junne. 2010. "Scale-Down Simulators for Metabolic Analysis of Large-Scale Bioprocesses." *Current Opinion in Biotechnology* 21, no. 1: 114–121. https://doi.org/10.1016/j.copbio.2010.02.001.

Olughu, W., G. Deepika, C. Hewitt, and C. Rielly. 2019. "Insight Into the Large-Scale Upstream Fermentation Environment Using Scaled-Down Models." *Journal of Chemical Technology & Biotechnology* 94, no. 3: 647–657. https://doi.org/10.1002/jctb.5804.

Revilla, G., F. R. Ramos, M. J. Lópeznieto, E. Alvarez, and J. F. Martín. 1986. "Glucose Represses Formation of Delta-(L-Alpha-Aminoadipyl)-L-Cysteinyl-D-Valine and Isopenicillin N Synthase but Not Penicillin Acyltransferase in *Penicillium chrysogenum*." *Journal of Bacteriology* 168, no. 2: 947–952. https://doi.org/10.1042/bj3010367.

Shende, V. V., K. D. Bauman, and B. S. Moore. 2024. "The Shikimate Pathway: Gateway to Metabolic Diversity." *Natural Product Reports* 41, no. 4: 604–648. https://doi.org/10.1039/d3np00037k.

Skye, G. E., and I. H. Segel. 1970. "Independent Regulation of Cysteine and Cystine Transport in *Penicillium chrysogenum*." *Archives of Biochemistry and Biophysics* 138, no. 1: 306–318. https://doi.org/10.1016/0003-9861(70)90311-5.

Spann, R., J. Glibstrup, K. Pellicer-Alborch, et al. 2019. "CFD Predicted pH Gradients in Lactic Acid Bacteria Cultivations." *Biotechnology and Bioengineering* 116, no. 4: 769–780. https://doi.org/10.1002/bit.26868.

Steyer, J. T., D. J. Downes, C. C. Hunter, P. A. Migeon, and R. B. Todd. 2021. "Duplication and Functional Divergence of Branched-Chain Amino Acid Biosynthesis Genes in *Aspergillus nidulans*." *mBio* 12, no. 3: 0076821. https://doi.org/10.1128/mBio.00768-21.

Strassman, M., A. J. Thomas, L. A. Locke, and S. Weinhouse. 1956. "The Biosynthesis of Isoleucine." *Journal of the American Chemical Society* 78, no. 1: 228–232. https://doi.org/10.1021/ja01582a063.

Vardar, F., and M. D. Lilly. 1982. "Effect of Cycling Dissolved Oxygen Concentrations on Product Formation in Penicillin Fermentations." *European Journal of Applied Microbiology and Biotechnology* 14, no. 14: 203–211. https://doi.org/10.1007/bf00498464.

Wang, G., J. Chu, Y. Zhuang, W. van Gulik, and H. Noorman. 2019. "A Dynamic Model-Based Preparation of Uniformly-^{13}C-Labeled Internal Standards Facilitates Quantitative Metabolomics Analysis of *Penicillium chrysogenum*." *Journal of Biotechnology* 299: 21–31. https://doi.org/10.1016/j.jbiotec.2019.04.021.

Wang, G., C. Haringa, H. Noorman, J. Chu, and Y. Zhuang. 2020. "Developing a Computational Framework To Advance Bioprocess Scale-Up." *Trends in Biotechnology* 38, no. 8: 846–856. https://doi.org/10.1016/j.tibtech.2020.01.009.

Wang, S., P. Liu, W. Shu, et al. 2019. "Dynamic Response of *Aspergillus niger* to Single Pulses of Glucose With High and Low Concentrations." *Bioresources and Bioprocessing* 6: 1–14. https://doi.org/10.1186/s40643-019-0251-y.

Wang, G., W. Tang, J. Xia, J. Chu, H. Noorman, and W. M. van Gulik. 2015. "Integration of Microbial Kinetics and Fluid Dynamics Toward Model-Driven Scale-Up of Industrial Bioprocesses." *Engineering in Life Sciences* 15, no. 1: 20–29. https://doi.org/10.1002/elsc.201400172.

Wang, X., Q. Yang, C. Haringa, et al. 2024. "An Industrial Perspective on Metabolic Responses of *Penicillium chrysogenum* to Periodic Dissolved Oxygen Feast-Famine Cycles in a Scale-Down System." *Biotechnology and Bioengineering* 121, no. 10: 3076–3098. https://doi.org/10.1002/bit.28782.

Wang, G., J. Zhao, C. Haringa, et al. 2018. "Comparative Performance of Different Scale-Down Simulators of Substrate Gradients in *Penicillium chrysogenum* Cultures: The Need of a Biological Systems Response Analysis." *Microbial Biotechnology* 11, no. 3: 486–497. https://doi.org/10.1111/1751-7915.13046.

Weber, J., A. Kayser, and U. Rinas. 2005. "Metabolic Flux Analysis of *Escherichia coli* in Glucose-Limited Continuous Culture. II. Dynamic Response to Famine and Feast, Activation of the Methylglyoxal Pathway and Oscillatory Behaviour." *Microbiology* 151, no. 3: 707–716. https://doi.org/10.1099/mic.0.27482-0.

Wei, P., C. Haringa, L. M. Portela, and H. J. Noorman. 2023. "Metabolic-Fluid Dynamics Model Construction and Scale-Down Design for an Industrial *Penicillium chrysogenum* Fermentation With Combined Dissolved Oxygen and Glucose Concentration Dynamics." *Chemical Engineering Science* 276: 118770. https://doi.org/10.1016/j.ces.2023.118770.

White, R. L., E.-M. M. John, J. E. Baldwin, and E. P. Abraham. 1982. "Stoichiometry of Oxygen Consumption in the Biosynthesis of Isopenicillin From a Tripeptide." *Biochemical Journal* 203, no. 3: 791–793. https://doi.org/10.1042/bj2030791.

Wu, L., M. R. Mashego, J. C. van Dam, et al. 2005. "Quantitative Analysis of the Microbial Metabolome by Isotope Dilution Mass Spectrometry Using Uniformly ^{13}C-Labeled Cell Extracts as Internal Standards." *Analytical Biochemistry* 336, no. 2: 164–171. https://doi.org/10.1016/j.ab.2004.09.001.

Yang, Q., W. Lin, J. Xu, et al. 2022. "Changes in Oxygen Availability During Glucose-Limited Chemostat Cultivations of *Penicillium chrysogenum* Lead to Rapid Metabolite, Flux and Productivity Responses." *Metabolites* 12, no. 1: 45. https://doi.org/10.3390/metabo12010045.

Zhao, J., M. A. Muawiya, Y. Zhuang, and G. Wang. 2024. "Developing Rational Scale-Down Simulators for Mimicking Substrate Heterogeneities Based on Cell Lifelines in Industrial-Scale Bioreactors." *Bioresource Technology* 395, no. 1: 130354. https://doi.org/10.1016/j.biortech.2024.130354.

Supporting Information

Additional supporting information can be found online in the Supporting Information section.